DISSERTATIONS IN
HEALTH SCIENCES

Päivi Koskenkorva

Magnetic Resonance Imaging of Unverricht-Lundborg Disease (EPM1)

Publications of the University of Eastern Finland
Dissertations in Health Sciences

UNIVERSITY OF
EASTERN FINLAND

PÄIVI KOSKENKORVA

Magnetic Resonance Imaging of Unverricht-Lundborg Disease (EPM1)

To be presented by permission of the Faculty of Health Sciences,
University of Eastern Finland
for public examination in Auditorium 1, Kuopio University Hospital,
23 March 2012, at 12 noon

Publications of the University of Eastern Finland
Dissertations in Health Sciences
Number 97

Departments of Clinical Radiology and Neurology
Institute of Clinical Medicine
School of Medicine
Faculty of Health Sciences
University of Eastern Finland

Kuopio
2012

Kopijyvä
Kuopio, 2012

Distributor:
University of Eastern Finland
Kuopio Campus Library
P.O.Box 1627
FI-70211 Kuopio, Finland
http://www.uef.fi/kirjasto

ISBN (print): 978-952-61-0687-8
ISBN (pdf): 978-952-61-0688-5
ISSN (print): 1798-5706
ISSN (pdf): 1798-5714
ISSN-L: 1798-5706

Author's address: Department of Clinical Radiology
Kuopio University Hospital
KUOPIO
FINLAND

Supervisors: Professor Ritva Vanninen, Ph.D.
Department of Clinical Radiology
Institute of Clinical Medicine, School of Medicine
Faculty of Health Sciences, University of Eastern Finland
KUOPIO
FINLAND

Professor Reetta Kälviäinen, Ph.D.
Department of Neurology
Institute of Clinical Medicine, School of Medicine
Faculty of Health Sciences, University of Eastern Finland
KUOPIO
FINLAND

Reviewers: Professor Osmo Tervonen, Ph.D.
Department of Diagnostic Radiology
Institute of Clinical Medicine
University of Oulu
OULU
FINLAND

Docent Merja Soilu-Hänninen, Ph.D.
Department of Neurology
University of Turku
TURKU
FINLAND

Opponent: Docent Riitta Parkkola, Ph.D.
Department of Radiology
University of Turku
TURKU
FINLAND

Koskenkorva, Päivi
Magnetic Resonance Imaging of Unverricht-Lundborg disease (EPM1).
University of Eastern Finland, Faculty of Health Sciences,2012.
Publications of the University of Eastern Finland. Dissertations in Health Sciences Number 97. Year. 58 p.

ISBN (print): 978-952-61-0687-8
ISBN (pdf): 978-952-61-0688-5
ISSN (print): 1798-5706
ISSN (pdf): 1798-5714
ISSN-L: 1798-5706

ABSTRACT

Unverricht-Lundborg disease (EPM1), caused by mutations in the cystatin B gene *(CSTB)*, is an autosomal recessively inherited disorder. It is the most common form of progressive myoclonus epilepsy. The prevalence of EPM1 is increased particularly in Finland where it is 4:100 000, offering a unique opportunity to study a large patient population. EPM1 is characterized by stimulus-sensitive and action-activated myoclonus, tonic-clonic seizures and ataxia. During the first 5-10 years, the symptoms progress and stabilize thereafter. About one-third of the patients become severely incapacitated.

At the time of diagnosis, magnetic resonance imaging (MRI) of the brain is usually normal. Cerebral and cerebellar atrophy may develop subsequently. No large scale imaging studies of EPM1 have been reported thus far. The aim of this study was to explore whether advanced imaging techniques could reveal previously undetected morphological changes in the brains of patients with EPM1. The brains of altogether 62 patients with EPM1 were imaged with MRI and their findings were compared with those of healthy controls.

Voxel-based morphometry (VBM) revealed regional bilateral gray matter volume loss in the motor cortex and thalamus of patients with EPM1, consistent with the motor symptoms of the disease. In addition, thinning of the sensorimotor, visual and auditory cortices was found by applying cortical thickness analysis. Cortical thickness correlated negatively with age, the duration of EPM1, and the severity of myoclonus. The findings parallel the stimulus-sensitive nature of the symptoms in EPM1. Diffusion tensor imaging with tract-based spatial statistics revealed widespread changes both in the supratentorial and infratentorial white matter (WM) of patients with EPM1, consistent with chronic WM degeneration. Directional diffusivity parameters indicate that the WM changes may reflect axonal and myelin loss. When comparing the clinical and imaging findings of patients who are compound heterozygous for the dodecamer repeat expansion and the c.202C>T mutation in the *CSTB* gene with those of patients who are homozygous for the dodecamer repeat expansion, the age at onset of symptoms seemed to be earlier in the compound heterozygotes. Furthermore, their myoclonic symptoms seemed to be more severe and the epileptic seizures were more drug-resistant than those of the homozygous patients. No differences were found between the MRI findings of the two groups.

To summarize, previously undetected regional morphological changes in the brains of patients with EPM1 were discovered with modern imaging techniques. The changes are consistent with the clinical symptoms of EPM1, and combined with detailed neurophysiological evaluation, they offer new insight into the pathogenesis of EPM1.

National Library of Medical Classification: WL 385, WN 185
Medical Subject Headings: Unverricht-Lundborg Syndrome; Magnetic Resonance Imaging; Cystatin B/genetics; Myoclonic Epilepsies, Progressive; Mutation/genetics; Brain Mapping; Finland

Koskenkorva, Päivi
Unverricht-Lundborgin taudin (EPM1) magneettikuvantaminen.
Itä-Suomen yliopisto, Terveystieteiden tiedekunta, 2012.
Publications of the University of Eastern Finland. Dissertations in Health Sciences Number 97. Year. 58 p.

ISBN (print): 978-952-61-0687-8
ISBN (pdf): 978-952-61-0688-5
ISSN (print): 1798-5706
ISSN (pdf): 1798-5714
ISSN-L: 1798-5706

TIIVISTELMÄ

Unverricht-Lundborgin tauti (EPM1), on kystatiini B-geenin mutaatiosta aiheutuva peittyvästi periytyvä sairaus. Se on tavallisin etenevän myoklonusepilepsian muoto. EPM1:n esiintyvyys on lisääntynyt erityisesti Suomessa (4:100000) antaen ainutlaatuisen mahdollisuuden tutkia laajaa potilasjoukkoa. Taudin oireita ovat ulkoisten aistiärsykkeiden provosoimat myokloniat, toonis-klooniset epileptiset kohtaukset ja ataksia. Oireet etenevät ensimmäisten 5-10 vuoden aikana, jonka jälkeen ne yleensä tasoittuvat. Noin kolmanneksella potilaista toimintakyky huononee huomattavasti.

Diagnoosivaiheessa aivojen magneettikuvaus on yleensä normaali. Iso- ja pikkuaivojen atrofiaa voi myöhemmin kehittyä. Laajoja EPM1:tä käsitteleviä kuvantamistutkimuksia ei toistaiseksi ole raportoitu. Tutkimuksen tavoitteena oli selvittää, löytyykö modernien kuvantamismenetelmien avulla aiemmin tuntemattomia aivojen rakennemuutoksia EPM1-potilailla. Yhteensä 62 potilaalle tehtiin aivojen magneettikuvaus ja löydöksiä verrattiin terveisiin verrokkihenkilöihin.

Vokselipohjaisella analyysimenetelmällä (voxel-based morphometry) löydettiin motorisiin oireisiin sopien harmaan aineen volyymikatoa molemmin puolin EPM1-potilaiden motorisella aivokuorella ja talamuksissa. Lisäksi korteksin paksuusanalyysia käyttäen todettiin ohenemista sensorimotorisella, näkö- ja kuuloaivokuorella. Aivokuoren oheneminen korreloitui käänteisesti ikään, sairastamisaikaan ja myoklonian vaikeusasteeseen. Löydökset sopivat oireisiin liittyvään ärsykeherkkyyteen. Vokselipohjaisella menetelmällä (tract-based spatial statistics) analysoituna diffuusiotensorikuvauksessa todettiin potilailla laaja-alaisia muutoksia sekä iso- että pikkuaivojen valkeassa aineessa krooniseen rappeumaan sopien. Diffuusion suuntaa kuvaavat parametrit osoittivat, että muutokset voivat liittyä aksoni- ja myeliinikatoon. Verrattaessa kliinistä taudinkuvaa ja kuvantamislöydöksiä todettiin, että taudin alkamisikä näytti olevan varhaisempi niillä potilailla, jotka ovat yhdistelmäheterotsygootteja valtamutaation ja harvinaisemman mutaation suhteen, kuin potilailla, joilla on pelkkä valtamutaatio kystatiini B-geenissä. Samoin myokloniset oireet näyttivät olevan heillä vaikeampia ja lääkevaste epileptisiä kohtauksia vastaan huonompi. Kuvantamislöydöksissä ei ryhmien välillä ollut eroja.

Moderneja kuvantamismenetelmiä käyttäen todettiin siis oireita selittäviä aivojen rakennemuutoksia EPM1-potilailla. Yhdistettynä neurofysiologisiin tutkimuksiin muutokset antavat uutta tietoa sairauden syntymekanismeista.

Yleinen suomalainen asiasanasto: epilepsia; magneettitutkimus – aivot; kuvantaminen – lääketiede

Acknowledgements

This thesis is based on a work carried out in the Department of Clinical Radiology in collaboration with the Department of Neurology, Kuopio University Hospital during the years 2006 - 2012.

I owe my deepest gratitude to Professor Ritva Vanninen, my principal supervisor. I am impressed by her efficiency both in clinical work and research. Her constant support during this project has been extremely important to me. One could not hope for better guidance and supervision.

I wish to express my warm gratitude to my supervisor, Professor Reetta Kälviäinen. Her enthusiastic attitude towards epilepsy research and her work at the Kuopio Epilepsy Center is truly admirable. Her expertise in neurology has been invaluable during this work.

I want to thank Professor Hannu Manninen, the Head of the Department of Radiology, for his favourable attitude towards research projects and for providing excellent facilities for both clinical work and research.

I am thankful to Professor Esa Mervaala for his knowledge of clinical neurophysiology and for his advice and guidance whenever needed.

I am grateful to Professor Anna-Elina Lehesjoki for her contribution to this thesis and for her valuable help with the mysteries of genetics which were not that familiar to me as a radiologist. She has always had time to answer my questions.

I wish to offer my sincere thanks to Professor Olli Gröhn and Professor Hilkka Soininen for their collaboration in this work.

I am greatly indebted to physicists Eini Niskanen, Ph.D and Mervi Könönen, M.Sc for all their help during this work. Eini has patiently taught me the principals of VBM analysis and has performed the cortical thickness analyses in this thesis. Her "image machine" has produced many of the excellent images in this study. Mervi has always had time to solve the problems I have faced during clinical and research work.

My warmest thanks belong to my co-workers; Jelena Hyppönen, Ph.D, who has collected the clinical data of the patients in the study; MR scientist Kimmo Lehtimäki for his help and co-operation with the TBSS work in this study; Otto Manninen, M.Sc, for his collaboration with our joint study "of mice and men"; neuropsychologist Marja Äikiä, Ph.D, who performed the neuropsychological tests and interpreted the data; and neuropediatricians Kai Eriksson, Ph.D and Tuula Kiviranta, Ph.D for their constructive comments about the work.

I owe my warmest gratitude to my colleagues Paula Bendel, Ph.D and Anna Sutela, Ph.D for their friendship and practical advice about scientific research. Paula and I learned the secrets of VBM and wrote our VBM work together. Her enthusiasm towards clinical work is inspiring. Anna has been my "room mate" at work for several years and we have shared the joys and sorrows of life.

I express my gratitude to Docent Merja Soilu-Hänninen and Professor Osmo Tervonen, the official referees of my thesis, for their thorough review and constructive criticisms.

I wish to express my warmest thanks to my fellow neuroradiologists Juhana Hakumäki, Ph.D., Aki Ikonen, M.D., Sanna Keränen, M.D., Antti Lehtimäki, M.D. and Teppo Mäkelä, M.D., for their invaluable professional comments and their patience for doing all the clinical work while I have been on research leave.

I wish to thank all my colleagues in the Department of Clinical Radiology for their company and interest in my work. I also owe my warm thanks to the skilful personnel of our department, especially in the MR unit: Kaija Räisänen, Kirsti Ritvanen and all the other radiographers who have patiently imaged the patients in this study.

Tuula Bruun and Taina Airola have given their invaluable secretarial help whenever needed, for which I express my sincere thanks.

I thank all the EPM1 patients who have participated in this study.

I am grateful to Nick Hayward, Ph.D., and Dr Ewen MacDonald, D. Pharm. for revising the English language of the manuscripts and the thesis.

My dearest thanks I dedicate to my parents Marjatta and Juho Koskenkorva for their loving support during my life. I also want to thank my "little sister" Johanna and her family, Tatu and Antti, for their friendship and company.

Finally, I thank the men in my life, Pekka, Juho and Ville, for keeping my mind off work and for reminding me of what is important in life.

This study was financially supported by Kuopio University Hospital (grant number 5772751), the Vaajasalo Foundation, the Academy of Finland, the Finnish Cultural Foundation of Northern Savo, the Radiological Society of Finland, Neuroradiologists of Finland and UCB Pharma SA.

Kuopio, February 2012

Päivi Koskenkorva

List of the original publications

This dissertation is based on the following original publications, which are referred to in the text by their Roman numerals:

I Koskenkorva P, Khyuppenen J, Niskanen E, Könönen M, Bendel P, Mervaala E, Lehesjoki A E, Kälviäinen R, Vanninen R. Motor cortex and thalamic atrophy in Unverricht-Lundborg disease: Voxel-based morphometric study. *Neurology 73: 606-611, 2009.*

II Koskenkorva P, Niskanen E, Hyppönen J, Könönen M, Mervaala E, Soininen H, Kälviäinen R, Vanninen R. Sensorimotor, visual and auditory cortical atrophy in Unverricht-Lundborg disease (EPM1) mapped with cortical thickness analysis. *AJNR Am J Neuroradiol.* 2012 Jan 19. [Epub ahead of print].

III *Manninen O, *Koskenkorva P, Lehtimäki K K, Hyppönen J, Könönen M, Laitinen T, Kalimo H, Kopra O, Kälviäinen R, Lehesjoki A E, Gröhn O, Vanninen R. Widespread white matter degeneration in Unverricht-Lundborg disease: Translational study in patients and *Cstb*-deficient mice using diffusion tensor imaging with tract-based spatial statistics. Submitted.

* Authors with equal contribution

IV Koskenkorva P, Hyppönen J, Äikiä M, Mervaala E, Kiviranta T, Eriksson K, Lehesjoki A E, Vanninen R, Kälviäinen R. Severer phenotype in Unverricht-Lundborg disease (EPM1) patients compound heterozygous for the dodecamer repeat expansion and the 202>T mutation in the *CSTB* gene. *Neurodegenerative Diseases 8: 515-522, 2011.*

Contents

Abbreviations

AD	axial diffusion
ADC	apparent diffusion coefficient
AED	antiepileptic drug
BOLD	blood oxygen level dependent
CSF	cerebrospinal fluid
CSTB	cystatin-B
CSTB	cystatin B gene
cstb-/-	cystatin B-deficient
CTH	cortical thickness
DTI	diffusion tensor imaging
DWI	diffusion weighted imaging
EPM1	Unverricht-Lundborg disease, progressive myoclonic epilepsy type I
FA	fractional anisotropy
FDR	false discovery rate
FLAIR	fluid attenuated inversion recovery
fMRI	functional magnetic resonance imaging
FUS	fused in sarcoma
FEW	family-wise error
GM	gray matter
GMS	gray matter surface
ICV	intracranial volume
JME	juvenile myoclonus epilepsy
MD	mean diffusion
MEG	magnetoencephalography
MERRF	myoclonic epilepsy with ragged red fibers
MNI	Montreal Neurological Institute
MPRAGE	magnetization prepared rapid acquisition gradient echo
MRI	magnetic resonance imaging
MRS	magnetic resonance spectroscopy
MV	multi-voxel
NCL	neuronal ceroid lipofuscinosis
PET	positron emission tomography
PIQ	performance intelligence quotient
PME	progressive myoclonus epilepsy
RD	radial diffusion
ROI	region of interest
SEF	somatosensory evoked fields

SEP	somatosensory evoked potentials
SII	secondary somatosensory cortex
SPECT	single photon emission computed tomography
SV	single voxel
TBSS	tract-based spatial statistics
TDP-43	TARDNA binding protein 43
TE	echo time
TMS	transcranial magnetic stimulation
TR	repeat time
UMRS	Unified Myoclonus Rating Scale
WAIS-R	Wechsler Adult Intelligence Scale Revised
VBM	voxel-based morphometry
VIQ	verbal intelligence quotient
WM	white matter
WMS	white matter surface

1 Introduction

Progressive myoclonus epilepsies (PME) constitute a heterogeneous group of diseases characterized by myoclonus, epileptic seizures and progressive neurological deterioration (Genton *et al.* 2005). Unverricht-Lundborg disease or progressive myoclonic epilepsy type 1 (EPM1, OMIM254800), which is an autosomal recessively inherited disorder, is the most common form of PME. It is caused by mutations in the cystatin B gene *(CSTB)* (Pennacchio *et al.* 1996), but the pathological basis for the disease remains unclear. The prevalence of EPM1 is increased in certain populations, particularly in Finland where it is 4:100 000 (Kälviäinen *et al.* 2008), offering a unique opportunity to study a large patient population of this rare condition.

At the time of diagnosis, magnetic resonance imaging (MRI) of the brain is usually normal in EPM1. Cerebral and cerebellar atrophy may develop subsequently. Loss of volume of the pons and cerebellum has been observed (Mascalchi *et al.* 2002). However, no large scale quantitative MRI studies of EPM1 have yet been reported. The development of MRI techniques enables a more detailed investigation of brain pathology in vivo than previously has been possible. The aim of the present study was to explore whether advanced MRI techniques would reveal previously undetected morphological changes in the brains of patients with EPM1 and provide more information about the pathophysiology of Unverricht-Lundborg disease.

2 Review of the literature

2.1 PROGRESSIVE MYOCLONUS EPILEPSIES

Progressive myoclonus epilepsies (PMEs) are a heterogeneous group of rare neurological disorders characterized by myoclonus, epilepsy, and progressive neurological deterioration, typically with cerebellar signs and dementia (Genton *et al.* 2005). They are genetic disorders; most are autosomal recessive, one is mitochondrial. The age of onset, presenting symptoms, predominance of symptoms as seizures, or myoclonus over cerebellar signs and dementia vary substantially across the different disorders and the different phenotypes may guide the clinician to the most likely cause. There are five main causes of PME: Unverricht-Lundborg disease, Lafora disease, neuronal ceroid lipofuscinoses (NCL), sialidoses, and myoclonic epilepsy with ragged red fibers (MERRF). These disease entities have been more accurately defined with recent advances in genetic studies (Shahwan *et al.* 2005, Shields 2004).

2.2 UNVERRICHT-LUNDBORG DISEASE (EPM1)

The most common cause of PME is Unverricht-Lundborg disease (progressive myoclonic epilepsy type 1, EPM1, OMIM254800). It is an autosomal recessively inherited disorder that was first described by Unverricht in 1891 (Unverricht 1891) and by Lundborg in 1903 (Lundborg 1903). The incidence of EPM1 in Finland is about 1:20 000 births per year (Norio *et al.* 1979), i.e. the highest reported. Currently there are about 200 diagnosed cases in Finland, and about three new cases are diagnosed each year (Kälviäinen *et al.* 2008). There is also a cluster of EPM1 in the Mediterranean (i.e. in Italy, certain locations of Southern France and in the North African countries of Tunisia, Algeria and Morocco) (Genton *et al.* 1990, Moulard *et al.* 2002). Sporadic cases are found worldwide and EPM1 is probably underdiagnosed in many countries (Eldridge *et al.* 1983, Lehesjoki *et al.* 1993, de Haan *et al.* 2004).

2.2.1 Clinical picture of EPM1

The age at onset of symptoms is usually between six and sixteen years (Genton *et al.* 2005). In at least half of patients, stimulus-sensitive or action-activated myoclonic jerks are the first symptoms (Norio *et al.* 1979, Koskiniemi *et al.* 1974a). The myoclonic jerks may be provoked by various stimuli such as light, physical exertion, noise and stress. They may be focal or multifocal and may generalize to a series of myoclonic seizures or even status myoclonicus (Genton *et al.* 2005, Kälviäinen *et al.* 2008). During the first five to ten years, the symptoms progress and stabilize thereafter (Magaudda *et al.* 2006). About one-third of patients become severely incapacitated (wheelchair bound, unable to eat and drink without help) (Kälviäinen *et al.* 2008).

Tonic-clonic seizures are another presenting symptom in almost half of patients (Norio *et al.* 1979, Koskiniemi *et al.* 1974a). Absence seizures may also be observed. Epileptic seizures are usually infrequent in the early stages of the disease, but they often increase in frequency during the following three to seven years. They may cease entirely with appropriate antiepileptic drug treatment (Kälviäinen *et al.* 2008). In rare cases, tonic-clonic seizures do not occur.

Some years after the disease onset, ataxia, loss of coordination, intention tremor and dysarthria usually develop. Individuals with EPM1 are mentally alert but show emotional

lability, depression and mild cognitive decline over time (Genton *et al.* 2005, Koskiniemi *et al.* 1974a).

The course of the disease is progressive, but naturally the phenotype of EPM1 is more heterogeneous than previously assumed. Some of the patients become wheelchair bound, whilst there also seems to be cases, whereby the myoclonus is so mild that it leads to a marked delay in the diagnosis, or a misdiagnosis of focal epilepsy or juvenile myoclonic epilepsy. The severity of the symptoms and the speed of disease progression can vary significantly even within the same family (Genton *et al.* 2005, Kälviäinen *et al.* 2008).

In the past, the life span of individuals with EPM1 was shortened and many died before 30 years of age (Koskiniemi *et al.* 1974a). Early or unexpected deaths of EPM1 patients have also been reported quite recently (Khiari *et al.* 2009). However, with advances in pharmacological, rehabilitative and psychosocial supportive treatment, most patients now live into their sixties or seventies (Kälviäinen *et al.* 2008).

Pharmacological treatment is mainly directed against epileptic seizures and myoclonus. Valproic acid is the first antiepileptic drug (AED) of choice. It diminishes myoclonus and the frequency of generalized seizures. It is usually combined with clonazepam. High-dose piracetam has also been found to be useful in the treatment of myoclonus. Levetiracetam seems to be effective for both myoclonus and generalized seizures. As add-on treatments, topiramate and zonisamide may also be used (Genton *et al.* 2005, Kälviäinen *et al.* 2008). The epileptic seizures can usually be controlled with pharmacological treatment, but the myoclonus can be quite debilitating despite extensive AED treatment. Phenytoin, including fosphenytoin in the acute setting, should not be used as it has been found to have side-effects that aggravate the neurological symptoms and may promote cerebellar degeneration (Eldridge *et al.* 1983). Sodium channel blockers and GABAergic drugs such as gabapentin and pregabalin should also be avoided as they may exacerbate myoclonus (Medina *et al.* 2005).

2.2.2 Diagnosis of EPM1

2.2.2.1 Clinical diagnosis

The diagnosis of EPM1 can be suspected when a previously healthy and normally developed child aged from 6 to 16 years presents with more than one of the following symptoms or signs:

1) Involuntary, stimulus or action-activated myoclonic jerks, or both
2) Generalized tonic-clonic seizures
3) Mild neurological signs in gross motor function (e.g. clumsiness) or in coordination tests (e.g. mild dysmetria) or in walking (e.g. mild ataxia)
4) Marked photosensitive, generalized spike-and-wave and polyspike-and-wave paroxysms in EEG (Koskiniemi *et al.* 1974b). The EEG background activity varies from normal to mildly slowed, remaining stable over time (Ferlazzo *et al.* 2007).
5) Signs of cortical or central atrophy (or both) on magnetic resonance imaging (MRI) of the brain, or normal MRI
6) A gradual worsening of myoclonus and ataxia

To establish the extent of the disease, a complete neurological examination is essential. Myoclonus should be evaluated at rest, with action, and in response to stimuli. EEG should be evaluated before any antiepileptic drug therapy is initiated, when it is most characteristic. The clinical diagnosis can be further supported and confirmed with genetic testing for the mutation in the cystatin B gene (Genton *et al.* 2005, Kälviäinen *et al.* 2008).

2.2.2.2 Genetic diagnosis

EPM1 is autosomal recessively inherited. The cystatin B gene *(CSTB)* is the only gene known to be associated with EPM1 (Pennacchio *et al.* 1996). It encodes cystatin B (CSTB), a

cysteine protease inhibitor. Human CSTB consists of 98 amino acids and it is widely expressed in different tissues and cell types. Although CSTB has been characterized in detail in vitro, its physiological function is still unknown (Joensuu *et al.* 2008).

Eleven different mutations in *CSTB* have been reported to underlie EPM1 (Joensuu *et al.* 2008, Erdinc *et al.* 2010). An expanded dodecamer repeat mutation is found in approximately 90% of the disease alleles worldwide (Lafreniere *et al.* 1997, Lalioti *et al.* 1997a, Virtaneva *et al.* 1997). It is detected in homozygous form in the majority of EPM1 patients. In the remaining patients the dodecamer repeat expansion mutation occurs in compound heterozygous form with one of the nine other mutations associated with EPM1 (Joensuu *et al.* 2008). No correlation has been found between the number of repeats and the severity of the disease or the age at onset so far (Virtaneva *et al.* 1997, Lalioti *et al.* 1997b, Lalioti *et al.* 1998). Reduced *CSTB* gene and protein expression is the primary pathological consequence in the majority of EPM1 mutations (Joensuu *et al.* 2008).

In addition to confirming the EPM1 diagnosis, genetic testing of the *CSTB* gene can be used for carrier testing and prenatal diagnosis.

2.2.2.3 Diagnostic imaging of EPM1

At the time of diagnosis the imaging findings of the brain are usually normal. Cerebral or cerebellar atrophy may develop subsequently. Loss of bulk of the pons, medulla and cerebellar hemispheres have all been reported in a study of ten patients with EPM1 (Mascalchi *et al.* 2002), otherwise imaging findings have been unspecific (Parmeggiani *et al.* 1997, Santoshkumar *et al.* 2008, Chew *et al.* 2008). Thickening of the skull has also been reported (Koskiniemi *et al.* 1974a, Korja *et al.* 2007a).

2.2.2.4 Differential diagnosis

If action myoclonus is absent or very mild at the onset of symptoms, a patient can easily be misdiagnosed as suffering from juvenile myoclonic epilepsy (JME). Individuals with JME have a normal neurological examination. EEG findings can be fairly similar to those seen in EPM1, although in EPM1 there is often background slowing. Myoclonic as well as tonic-clonic seizures are present with both conditions. The distinctive symptom in EPM1 is action myoclonus, which may only become clearly evident even years after the onset of symptoms (Kälviäinen *et al.* 2008). In cases of severe progression particularly of cognitive or visual symptoms, other forms of PME should be considered (Kälviäinen *et al.* 2008, Shahwan *et al.* 2005). A disorder with an EPM1-like phenotype with linkage to chromosome 12 has been reported, but the causative gene is unknown (Berkovic *et al.* 2005). In *CSTB* mutation-negative cases this disorder should be considered.

2.2.3 Histopathological findings in EPM1

The histopathological findings in EPM1 are limited. They consist of loss of cerebellar granule and Purkinje cells, degeneration and loss of neurons in the cerebral cortex, striatum, thalamus, brainstem nuclei and spinal motor neurons (Eldridge *et al.* 1983, Koskiniemi *et al.* 1974a, Haltia *et al.* 1969, Cohen *et al.* 2011). Recently neuronal cytoplasmic inclusions containing the lysosomal proteins cathepsin B and CD68 have been identified. These inclusions also showed immunopositivity to both TDP-43 and FUS, associated in some cases with an absence of normal neuronal nuclear TDP-43 staining. TDP-43 and FUS are proteins that are encoded by the genes *TARDBP* and *FUS* in humans. Mutations in these genes have been associated with neurodegenerative disorders such as frontotemporal lobar degeneration and amyotrophic lateral sclerosis (ALS). This finding is consistent with neurodegeneration in EPM1A as at least a partial consequence of lysosomal damage to neurons, which have reduced CSTB-related neuroprotection (Cohen *et al.* 2011).

2.2.4 Animal model of EPM1

A Cstb-deficient (*Cstb*-/-) mouse model has been generated to study EPM1. The model mimics the human phenotype reasonably well. The *Cstb*-/- mice feature myoclonic seizures that develop by one month of age, and progressive ataxia that becomes evident by six months of age. However, in *Cstb*-/- mice the myoclonic seizures occur during sleep, whereas in humans they are action-activated and stimulus sensitive. Furthermore, no tonic-clonic seizures, photosensitivity or spike-wave complexes in EEG have been observed in mice (Pennacchio *et al.* 1998).

Histopathological findings in *Cstb*-/- mice consist of severe loss of cerebellar granule cells due to apoptotic death (Pennacchio *et al.* 1998). Less marked neuronal apoptosis can be seen in the hippocampal formation and entorhinal cortex of animals aged 2-4 months. In older mice, there is gliosis in the hippocampal formation, entorhinal cortex, neocortex and the striatum. There is also widespread gliosis in the white matter (Shannon *et al.* 2002). Many of these histological features parallel the findings in humans.

2.3 ADVANCED MR IMAGING OF THE BRAIN

2.3.1 Clinical MR imaging

Magnetic resonance imaging (MRI) is a method of choice for imaging disorders of the central nervous system, particularly epilepsy and neurodegeneration. Compared with x-ray computed tomography (CT), MRI offers superior tissue contrast and eliminates the effect of artifacts caused by bone structures, especially in the posterior fossa. Furthermore, MRI enables imaging in multiple planes and thin slices, and it does not use ionizing radiation. However, a longer scanning time makes MRI more susceptible to motion artifacts and thus the imaging of patients who are restless or suffer from movement disorders can be challenging. There are also some contraindications to MRI: patients with cardiac pacemakers, cochlear implants, implanted neurostimulators, older ferromagnetic aneurysm clips, or metal in the eye cannot be imaged with MRI (Shellock *et al.* 1993).

2.3.2 Volumetric MR imaging

In recent years volumetric MR imaging has become a widely used tool to study alterations of brain volumes in neurodegenerative disorders such as Alzheimer's disease (Teipel *et al.* 2008) or multiple sclerosis (Sicotte *et al.* 2008), but it has also been used in studies of epilepsy (Betting *et al.* 2010), some cerebrovascular disorders (Bendel *et al.* 2009) and psychiatric disorders (Yoshida *et al.* 2009). There are several methods for volumetric MR imaging of the brain. Most of them utilize high-resolution T1-weighted three-dimensional imaging. Analyses can be performed by manually or semi-manually outlining regions of interest (ROI), but this is time consuming, operator dependent, and requires a predefined ROI. Techniques for studying whole brain volumes in an automated manner have therefore been developed, including deformation-based morphometry (DBM) (Ashburner *et al.* 1998), tensor-based morphometry (TBM) (Good *et al.* 2001b), voxel-based morphometry (VBM) (Ashburner *et al.* 2000, Good *et al.* 2001a) and methods for measuring cortical thickness (MacDonald *et al.* 2000).

2.3.2.1 Manual volumetry

Manual volumetric methods are considered as the gold standard for examining structural volumes of the brain. Manual volumetry has been utilized for instance in studies of neurodegeneration (Mascalchi *et al.* 1998b, Soininen *et al.* 1994) and epilepsy (Bernasconi *et al.* 2003). The ROI is manually drawn in consecutive MRI slices covering the anatomical structure in question, and the volume is determined by summing up the voxels in the ROI across all slices and then multiplying the structure area by the sum of the section and gap

thicknesses. Nowadays commercial, semi- and fully automatic methods have been developed (Bendel *et al.* 2006, Wolz *et al.* 2011, Lötjönen *et al.* 2011).

2.3.2.2 Voxel-based morphometry

Voxel-based morphometry (VBM) is an established and widely published method. It has been applied to several conditions such as neurodegeneration (Hamalainen *et al.* 2007b, Mezzapesa *et al.* 2007, Beyer *et al.* 2007), JME (Kim *et al.* 2007), temporal lobe epilepsy (Focke 2008), and psychosis (Spencer *et al.* 2007). VBM provides an automated whole brain method to study estimated gray matter (GM) concentration surrounding a given voxel. It can also be utilized to analyze changes in white matter (WM) or cerebrospinal fluid (CSF), and it is possible to compare brain volume changes within the same study population in longitudinal studies. The primary VBM steps include normalization of the original MR images into the same stereotactic space, segmentation of normalized images into GM, WM and CSF compartments, modulation of the gray matter images in order to keep the total amount of GM volume in normalized images the same as it was in the original images, and smoothing of modulated images (Ashburner *et al.* 2000). In the optimized VBM method additional preprocessing steps are employed to exclude non-brain voxels prior to normalization and subsequent segmentation, thus increasing the validity of the results (Good *et al.* 2001a). Statistical analyses of regionally specific between group differences in GM volumes are assessed using standard parametric tests like t-tests or F-tests (Ashburner *et al.* 2000). The Montreal Neurological Institute (MNI) coordinates for the peak voxels can be transformed into Talairach space using the mni2tal routine (http://www.mrc-cbu.cam.ac.uk/imaging/index.html). The anatomical locations of the peak voxels in the significant clusters are determined using the Talairach Applet (Lancaster *et al.* 2000) and further verified from anatomical atlases (Duvernoy 1999, Tamraz 2006).

2.3.3 Cortical thickness analysis

Cortical thickness analysis is a novel method that has been proposed as a more sophisticated alternative to volumetric and voxel-based morphometry (VBM) methods to measure regional brain atrophy (Lerch *et al.* 2005b). This method has been shown to be reliable in detecting changes in cortical morphology both at the single subject level and at the group level, and it provides a direct quantitative measure of the thickness of the cerebral cortex (Lerch *et al.* 2005a). It has shown promise as a sensitive imaging biomarker in mild cognitive impairment and Alzheimer's disease, autism, and temporal lobe epilepsy (Julkunen *et al.* 2009, Hyde *et al.* 2010, Bernhardt *et al.* 2008). There are several methods to reconstruct the cortical surface, of which there are three that are more prominent (Kim *et al.* 2005, Fischl *et al.* 2000, Mangin *et al.* 1995). Generally, the processing sequence includes preprocessing steps such as spatial normalization, intensity homogeneity correction, skull stripping and tissue classification (Lee *et al.* 2006). Cortical thickness analysis involves multiple image processing steps, each method having its own procedure to create the cortical surface (Kim *et al.* 2005, Fischl *et al.* 2000, Mangin *et al.* 1995). Once the thickness maps have been generated, the statistical group analyses can be performed, for example, using the General Linear Model and the t-test corrected for multiple comparisons (Lerch *et al.* 2005a).

2.3.4 Diffusion weighted imaging

Diffusion weighted imaging (DWI) is sensitive to molecular diffusion, which is the result of the random thermal (Brownian) motion involving all molecules including water. DWI is based on a conventional spin-echo sequence with an additional gradient pulse applied between the initial 90° pulse and the refocusing 180° pulse. The gradient pulse causes a phase shift that is cancelled when a second gradient pulse is applied after the 180° pulse, if

no diffusion has occurred during the period between the two gradient pulses. However, if molecules have been displaced, the cancellation of the phase shifts will be incomplete, which is seen as decreased signal intensity. The amount of signal attenuation is exponentially dependent on the diffusion coefficient D and the strength and timing of the diffusion gradients, which are expressed as the constant b:

$$\text{Signal attenuation} \approx e^{-bD} \tag{2.1}$$

Thus, b gives the amount of diffusion weighting of the diffusion imaging spin-echo sequence and is calculated as:

$$b = \gamma^2 G^2 \delta^2 (\Delta - \delta/3) \tag{2.2}$$

where G is the gradient strength, δ is the duration of the gradient, Δ is the time between the onset of gradients, and γ is the gyromagnetic ratio of the hydrogen nucleus (Basser 2009).

In a diffusion weighted image the areas of restricted diffusion such as ischemic brain tissue, appear hyperintense in contrast to normal tissue. The mechanisms for this restricted diffusion include movement of water into the intracellular compartment, cell swelling resulting in a reduction of the extracellular space, and increased cytoplasmic viscosity (Yoo *et al.* 2011). In CSF the water molecules can move freely and thus it appears very hypointense in DW images. In addition to diffusion, other parameters such as "T2 shine-through" have an effect on the signal intensity in DW images. Quantification of the apparent diffusion coefficient (ADC) helps to distinguish between hyperintensity arising from true reduction in the ADC and that reflecting T2 prolongation. This requires the acquisition of images with two different b values. In ADC maps, each voxel gives the value of the ADC in tissue and restricted diffusion is seen as hypointensity, while CSF appears hyperintense. Thus, the diffusion differences in tissues are demonstrated without interference from T2 (Basser 2009, Roberts *et al.* 2007).

The ADC reflects the overall translational water motion. However, in the central nervous system (CNS) axonal membranes and myelin sheaths cause barriers to water displacement, so that water more readily diffuses parallel to white matter tracts than perpendicular to them. Consequently, the amount of diffusion is dependent on the direction of the diffusion gradient. To improve the accuracy of the ADC measurement, values derived from three orthogonal directions are used in standard practice. Thus, the value of any given voxel in the ADC or DW images represents the averaged values of the three gradient directions (Yang *et al.* 2011).

The principal clinical application for DWI is acute cerebral ischemia (Yoo *et al.* 2011), but today it is also increasingly utilized in tumor imaging (Hygino da Cruz *et al.* 2011), imaging of CNS infections (Gasparetto *et al.* 2011a) and traumatic brain injury (Gasparetto *et al.* 2011b). In addition, DWI has been utilized in head and neck imaging for detection of middle ear cholesteatoma (Yamashita *et al.* 2011).

2.3.4.1 Diffusion tensor imaging

Diffusion tensor imaging (DTI) has been used in several diseases to evaluate the integrity of the WM tracts *in vivo* (Deppe *et al.* 2008, Sage *et al.* 2007, Thivard *et al.* 2007, Damoiseaux *et al.* 2009, Liu *et al.* 2009). Diffusion anisotropy describes how variable the diffusion is in different directions. The most commonly used parameter to quantitate diffusion anisotropy is fractional anisotropy (FA), which is independent of local fiber orientation and can therefore be compared between subjects and groups. To determine the diffusion tensor, the diffusion must be measured in at least six different directions. From those it is possible to determine the degree and direction of anisotropy on a per-pixel basis (Roberts *et al.* 2007).

Information on directional diffusion can also be obtained from the three eigenvalues of the diffusion tensor ($\lambda_1, \lambda_2, \lambda_3$). λ_1 (axial diffusion, AD) reflects diffusion parallel to axonal fibers and $\lambda_2 + \lambda_3 / 2$ (radial diffusion, RD) reflects diffusion perpendicular to axonal fibers. Combined together, these measures reflect the cohesion of fibers within WM tracts (Pierpaoli *et al.* 1996). In animal studies, axonal damage has been reported to decrease AD markedly and RD insignificantly, whereas myelin injury increases RD without changing AD (Song *et al.* 2003, Song *et al.* 2005). The DTI data can be analyzed using either ROI-based methods or voxel-based methods that enable a whole brain approach. It is also possible to digitally reconstruct WM fiber paths with tractography (Mori *et al.* 1999).

2.3.4.2 ROI-based methods

In ROI-based methods the ROI is manually outlined and placed on the tract of interest in FA maps of individual patients, so the FA values are then measured from the ROI. Thus, these methods require a predefined region of interest, lacking whole brain volume information. In addition, it is often difficult to place ROIs on small or thin tracts objectively and accurately. Different voxel-based methods have been developed to overcome these problems.

2.3.4.3 Voxel-based methods

Voxel-based methods enable spatial localization of diffusion related changes in the whole brain. They are fully automated and simple to apply. Many studies follow an approach similar to that of voxel-based morphometry (Ashburner *et al.* 2000, Good *et al.* 2001c). VBM style analysis can be applied to FA images (Simon *et al.* 2005). Each subject's FA image is registered into a standard space and smoothed before voxelwise statistics are carried out. However, one cannot guarantee that any given structure has been aligned to the same structure in all the subjects, and that any voxel in standard space contains the same information from the same WM structure in every subject. Furthermore, the extent of smoothing can affect the results substantially (Jones *et al.* 2005), and there is no general agreement on how much smoothing is appropriate. Due to these limitations, there has been a need for more sophisticated approaches.

Tract-based spatial statistics (TBSS) analysis has been proposed as a solution to overcome the limitations of ROI-based and VBM style methods. In TBSS, the DTI data are projected on a common "FA-skeleton" of major white matter structures and smoothing is not required (Smith *et al.* 2006, Smith *et al.* 2007). TBSS has been used in studies of aging and dementia (Damoiseaux *et al.* 2009, Liu *et al.* 2009), temporal lobe epilepsy (Focke *et al.* 2008) and dyslexia (Richards *et al.* 2008). Briefly, the TBSS approach involves the following steps: A common registration target is identified and all subjects' FA images are aligned to this target using nonlinear registration. Perfect alignment is not required at this point. A mean FA image is then created using all aligned images and "thinned" to create a skeletonised FA image; a representation of the centers of WM tracts that are common to all subjects. Each subjects' aligned FA image is then projected onto the skeleton, and voxelwise statistics are carried out across subjects on the skeleton-space FA data (Smith *et al.* 2006).

2.3.5 Other MRI techniques

2.3.5.1 Proton MR spectroscopy

Proton MR spectroscopy (MRS) is a noninvasive technique that provides metabolic information about the brain. It is able to detect abnormalities before they are visible in structural MRI. Together with other MRI techniques, MRS can be helpful both in diagnostics and differential diagnostics of brain tumors (Weybright *et al.* 2005, Majos *et al.* 2009, Fellows *et al.* 2010), metabolic (Brandao *et al.* 2004) or degenerative (Mascalchi *et al.* 2002, Mascalchi *et al.* 1998a) diseases, or brain injury (Walz *et al.* 2008). Spectroscopic

information depends on the repetition time (TR) and the echo time (TE) employed, because cerebral metabolites have different T1 and T2 relaxation times. N-acetylaspartate (a neuronal marker), creatine (a marker of energy metabolism), choline (a marker of cell membrane proliferation) and lactate (a product of anaerobic glycolysis) can be identified with short and long TEs. Metabolites detected only with short TEs are lipids (products of brain destruction), glutamine and glutamate (neurotransmitters), and myo-inositol (a glial cell marker) (Brandao *et al.* 2004).

MRS can be performed with either single voxel (SV) or multivoxel (MV) techniques. In the SV technique, appropriate voxel positioning is critical. Voxels must be positioned away from sources of susceptibility artifacts and lipids. The data is usually acquired in 3 to 5 minutes. Restricted anatomical coverage is the main limitation of the SV technique. The signals are displayed as a spectral plot instead of an image (Brandao *et al.* 2004, Cousins 1995).

The MV technique (chemical shift imaging, magnetic resonance spectroscopic imaging) allows gathering data from multiple voxels simultaneously, providing information of the spatial distribution of the measured signal. MV analyses can be performed as two-dimensional or as three-dimensional studies. After quantification of the measured spectra, the results can be displayed as images of metabolite concentrations (Brandao *et al.* 2004, Skoch *et al.* 2008).

2.3.5.2 Functional MRI

Functional MRI (fMRI) is based on the blood oxygen level-dependent (BOLD) changes in MRI signal that arise when changes in neuronal activity occur following a change in brain state, which may be produced by a stimulus or a task. The BOLD contrast relies on changes in deoxyhemoglobin, which acts as an endogenous paramagnetic contrast agent. An increase in neural activity in a certain cortical region stimulates an increase in local blood flow in order to meet the larger demand for oxygen and other substrates. The change in regional blood flow exceeds the additional metabolic demand, so the concentration of deoxyhemoglobin within tissue decreases, resulting in a less rapid decay of the MRI signal from that region. Thus the signal is greater than that in other, less active areas of the brain. This small signal increase is the BOLD signal recorded in fMRI (Gore 2003, Kim *et al.* 2006). In fMRI, various kinds of stimuli are administered in a controlled fashion to the subject in the MR scanner. For example, sounds may be played or visual scenes may be presented, and small motor movements or responses can be recorded.

However, there can be situations where the stimuli cannot be successfully applied, e.g. the patient may suffer from movement disorder, paresis or paralysis or has attention deficit. Furthermore, appropriate MRI-compatible stimulus devices may not be available. In these cases, fMRI during a patient's rest is a useful application. Resting state fMRI is performed without tasks or external stimuli, thus requiring less cooperation from the patient. It is based on detecting the low-frequency fluctuations of the temporal BOLD signal in the resting brain (Biswal *et al.* 1995, Paakki *et al.* 2010, Kokkonen *et al.* 2009).

Functional MRI can be used for both clinical and research purposes. For instance, mapping of critical sensory and motor functions prior to neurosurgery is becoming an established application (Haberg *et al.* 2004, Kokkonen *et al.* 2009). fMRI has also been utilized in studies of neurodegeneration such as Alzheimer's disease (Hämäläinen *et al.* 2007a, Li *et al.* 2011). Recently some fMRI studies of EPM1 with a limited number of patients have been published (Visani *et al.* 2011, Visani *et al.* 2010, Manganotti *et al.* 2011).

2.4 POSITRON EMISSION TOMOGRAPHY (PET) AND SINGLE PHOTON EMISSION COMPUTED TOMOGRAPHY (SPECT)

Molecular imaging is not within the scope of this thesis. However, in many cases it offers complementary information to MR imaging, and in some cases when structural imaging is normal, molecular imaging can be of diagnostic value. Positron emission tomography (PET) enables tomographic imaging of local concentrations of injected biologically active, radioactively labeled substances. In PET, positron-emitting isotopes with short half-lives such as [^{15}O] (2 min), [^{11}C] (20 min) and [^{18}F] (110 min) are used. Thus the availability of PET is limited by the need for an on-site cyclotron to produce [^{15}O] and [^{11}C]. [^{18}F]-labeled substances can, however, be transported in from off-site.

Cerebral glucose metabolic mapping using PET and 2-[^{18}F]fluoro-2-deoxyglucose (FDG) has been extensively studied in epilepsy. In focal epilepsies, regions of interictal glucose hypometabolism are associated with seizure-generating sites in the brain. The pathophysiology of decreased [^{18}F]FDG activity interictally is, however, unknown. Interictal [^{18}F]FDG PET is clinically applied in planning resective epilepsy surgery (Henry *et al.* 2004).

Single photon emission computed tomography (SPECT) studies involve cerebral blood flow imaging using radiopharmaceuticals such as technetium-99m-hexamethylpropylene amine oxime (^{99m}Tc-HMPAO) or ^{99m}Tc-bicisate. SPECT can be used for peri-ictal imaging in patients with focal epilepsy being considered for surgery. Ictal SPECT studies have been useful to identify a region of focal hyperperfusion (Cascino *et al.* 2004).

PET and SPECT can also be utilized for the classification and differential diagnosis of neurodegenerative diseases e.g. parkinsonian syndromes (PS). The pathology in PS involves the dopaminergic system, of which PET and SPECT studies can offer valuable diagnostic information. Both pre and postsynaptic functions can be evaluated (Tatsch 2010). Furthermore, PET imaging with [^{18}F]FDG and Pittsburgh Imaging Compound B (PIB), can be applied to cognitive disorders such as Alzheimer disease (Scheinin *et al.* 2009).

3 Aims of the study

The general aim of the study was to explore whether advanced MRI techniques would reveal previously undetected morphological changes in the brains of patients with EPM1 compared with healthy controls.

The more specific aims were:

I: To evaluate if patients with EPM1 exhibit regional gray matter volume loss when compared with healthy age and gender matched controls by utilizing voxel-based morphometry (VBM).

II: To assess if there are regional alterations in cortical thickness of patients with EPM1 compared with healthy controls and to correlate the possible changes with clinical parameters by employing cortical thickness analysis.

III: To evaluate if patients with EPM1 exhibit white matter changes compared with healthy controls by using diffusion tensor imaging (DTI) with tract-based spatial statistics (TBSS).

IV: To evaluate the genotype-phenotype correlations in EPM1 patients who are compound heterozygous for the dodecamer repeat expansion and the c.202C>T mutation in the *CSTB* gene.

4 Patients and methods

4.1 STUDY DESIGN AND PATIENTS

The Ethical Committee of Kuopio University Hospital approved the study protocol and written informed consent was obtained from all participants. Genetically verified EPM1 patients participating in an ongoing clinical and molecular genetics study carried out by Kuopio Epilepsy Center, Kuopio University Hospital, jointly with the Folkhälsan Institute of Genetics and Neuroscience Center, University of Helsinki, were evaluated at Kuopio University Hospital between November 2006 and May 2009. The patients had either participated in an earlier molecular genetics study conducted by the study center or were referred to the center during the study. **Table 1** demonstrates the study design and patient flow for Studies I-IV. A total of 62 patients were studied. In studies I-III all patients were homozygous for the dodecamer repeat mutation in *CSTB*. In study IV, five patients were compound heterozygotes for the dodecamer repeat expansion and the c.202C>T mutation in the *CSTB* gene, and the control patients were homozygotes for the major mutation. The healthy control group consisted of volunteers matched for age and sex.

4.2 CLINICAL EVALUATION AND NEUROPHYSIOLOGY

A neurologist performed the clinical evaluations of patients with EPM1. Patients' medical histories were collected from medical records and by interviewing the patients and their relatives. A Unified Myoclonus Rating Scale (UMRS) test panel was performed as part of the clinical patient evaluation. UMRS is a quantitative 74-item clinical rating instrument comprising of 8 sections (Frucht *et al.* 2002). In the present study, three sections were used to evaluate the severity of myoclonus: Stimulus Sensitivity (maximum score 17), Myoclonus with Action (maximum score 160), and Functional Test (maximum score 28). These sections were video recorded and evaluated using a standard protocol (Frucht *et al.* 2002). Higher UMRS scores indicate more severe myoclonus.

A neurophysiologist re-evaluated all available EEG data based on reports and where possible, on original digital EEG recordings (Study IV).

Table 1. The study design.

Study	**Study purpose**	**Patients (n)**	**Controls (n)**	**Methods**
Study I	To evaluate possible regional gray matter volume loss in EPM1	34 homozygotes	30	MRI, voxel-based morphometry
Study II	To assess possible regional alterations in cortical thickness in EPM1	53 homozygotes	70	MRI, cortical thickness analysis
Study III	To evaluate possible white matter changes in EPM1	19 homozygotes	18	MRI, diffusion tensor imaging with tract-based spatial statistics
Study IV	To evaluate the genotype-phenotype correlations in EPM1	5 compound heterozygotes, 21 homozygotes	24	Clinical evaluation, neurophysiology, neuropsychology, MRI

4.3 NEUROPSYCHOLOGY (STUDY IV)

Detailed neuropsychological evaluation was performed by a neuropsychologist. The evaluation consisted of measures for intellectual ability, verbal learning and memory and visuomotor speed. On the basis of six subtests of the Wechsler Adult Intelligence Scale Revised (WAIS-R), Information; Similarities, Digit Span, Digit Symbol, Picture Completion and Block Design, Verbal and Performance Intellectual Quotients (VIQ and PIQ, respectively) were estimated (Wechsler 1981). Mild cognitive impairment was considered when the performance was more than 1 SD below the mean (IQ between 85 and 70), moderate when the performance was 2 SDs below the mean (IQ between 69 and 55) and severe when performance was 3 SDs below the mean (IQ less than 55). Verbal learning and memory were assessed with the List Learning Task which consisted of four learning trials of 15 unrelated words and the percent retention score of the learned words as a measure for delayed recall. Logical memory was evaluated with immediate and delayed recall of two stories, the second story was read two times. Percent retention scores of the story contents were calculated for the delayed memory. Visuomotor speed was evaluated with the Alternating S-task, in which the subject drew the letter 'S' and then a reversed letter 'S' alternately and continually for two minutes.

4.4 MR IMAGING

4.4.1 MRI protocol

All subjects underwent MR imaging (1.5 T, Siemens Avanto) including T1- and T2-weighted spin-echo sequences, a fluid-attenuated inversion recovery sequence (FLAIR), and T1-weighted three-dimensional (T1-3D) imaging (TR 1980 ms, TE 3.09 ms, flip angle 15°, matrix 256 x 256, 176 sagittal slices, slice thickness varying between 1.0 mm to 1.2 mm depending on the size of the head, and an in-slice resolution of 1.0 mm x 1.0 mm).

DTI data were collected using a gradient echo single shot EPI sequence (TE 98 ms, TR 12300 ms, matrix 128×128, FOV 256×256 mm^2, 73 axial slices, slice thickness 2 mm) with diffusion gradients (b-values 0 and 1000 s/mm^2) applied in 30 directions. For spectroscopy, 15 mm thick volumes of interest (VOI) were placed through the thalamus and basal ganglia, including surrounding temporoparietal white matter and occipital gray matter (80 x 80 mm). Water-suppressed spectra with a repetition time (TR) of 1,500 ms and echo times (TEs) of 30-270 ms to detect rapidly relaxing metabolites and noninverted lactate were obtained.

When preparing the patients for imaging, the atmosphere in the MR unit was kept as calm as possible. Given the stimulus-sensitive myoclonic symptoms in EPM1, a scanning time of one hour was arranged for each patient in order to minimize the possibility of motion artifacts in the MR images. To prevent the loud noise of the MR scanner from triggering myoclonic jerks, some of the patients used hearing protectors in addition to ear plugs. Motion correction software was available if necessary.

4.4.2 MRI analysis

A neuroradiologist assessed all conventional images visually for focal abnormalities. Presence of possible brain atrophy was visually evaluated (Study I) on a four-point scale (0 = no atrophy; 1 = mild; 2 = moderate; 3 = severe). Presence of white matter lesions (Study III) was assessed using the Fazekas classification (Fazekas *et al.* 1987).

4.4.3 Voxel-based morphometry (Studies I and IV)

T1-3D images were processed using optimized voxel-based morphometry (VBM) (Ashburner *et al.* 2000, Good *et al.* 2001a) with VBM2-toolbox (http://dbm.neuro.uni-

jena/vbm/) in SPM2 (Wellcome Department of Imaging Neuroscience, London, UK; www.fil.ion.ac.uk/spm) running under Matlab 6.5 (MathWorks, Inc.). The procedure includes generation of a customized template and prior probability maps and the primary VBM steps: normalization of the original MR images, segmentation of normalized images, modulation of the gray matter (GM) images in order to keep the total amount of GM volume in normalized images the same as it was in the original images, and smoothing of modulated images.

First, a customized template of the whole brain and prior probability maps (priors) were created using all study participants. The origin of spatial coordinates in the individual images was manually set to the anterior commissure and images were reoriented perpendicular to the intercommissural line. All images were then spatially normalized to the Montreal Neurological Institute (MNI) template provided in SPM2 using a 12 parameter affine transformation; segmented into GM, white matter (WM), and cerebrospinal fluid (CSF) compartments; smoothed with an 8 mm Gaussian filter; and averaged to obtain customized priors.

Next, the primary VBM steps were performed. The original images were segmented, and parameters for normalization were determined. The absolute volumes of GM, WM, and CSF were calculated from the segments and further summarized to obtain the total intracranial volume (ICV); the CSF/ICV ratio was calculated from these values. Using the estimated normalization parameters, the original images were normalized to the customized template through affine and non-linear transformations, resampling to 1 x 1 x 1 mm, and using no masking. The normalized images were then segmented into GM, WM, and CSF using the customized priors. Finally, a modulation was performed on the segmented GM images by multiplying the GM voxels by the Jacobian determinants derived from the spatial normalization step. The modulated GM images were smoothed with a 12 mm Gaussian kernel. The procedure of VBM is demonstrated in **Figure 1**.

Regionally specific differences in GM volume between patients and controls (Study I) were assessed using an analysis of covariance with age, sex, and total intracranial volume (calculated as the sum of GM, WM and CSF volumes) treated as confounding covariates. Between group differences were analyzed using a t-test with a height threshold of $p<0.05$ corrected with the family-wise error method. Clusters exceeding 50 edge-connected voxels were included in the reported analysis. The MNI coordinates for the peak voxels were transformed into Talairach space using the mni2tal routine (http://www.mrc-cbu.cam.ac.uk/imaging/index.html). The anatomical locations of the peak voxels in the significant clusters were found using the Talairach Applet (Lancaster *et al.* 2000) and further verified from an anatomical atlas (Duvernoy 1999).

To study the differences in GM volumes between the compound heterozygous patients and healthy controls (study IV), a region of interest (ROI) analysis based on the areas of GM volume loss found in study I of EPM1 patients homozygous for the expansion mutation in *CSTB* (primary and supplementary motor areas and thalami) was performed. ROIs were manually traced on a study-specific mean image with MriCro (http://www.sph.sc.edu/comd/rorden/mricro.html). A similar ROI analysis was performed between the compound heterozygotes and the homozygous patients. Regionally specific differences in GM volume between the study groups were assessed using an analysis of covariance with age, sex and total intracranial volume treated as confounding covariates with a threshold of $p<0.02$ corrected with the false discovery rate method (Genovese *et al.* 2002).

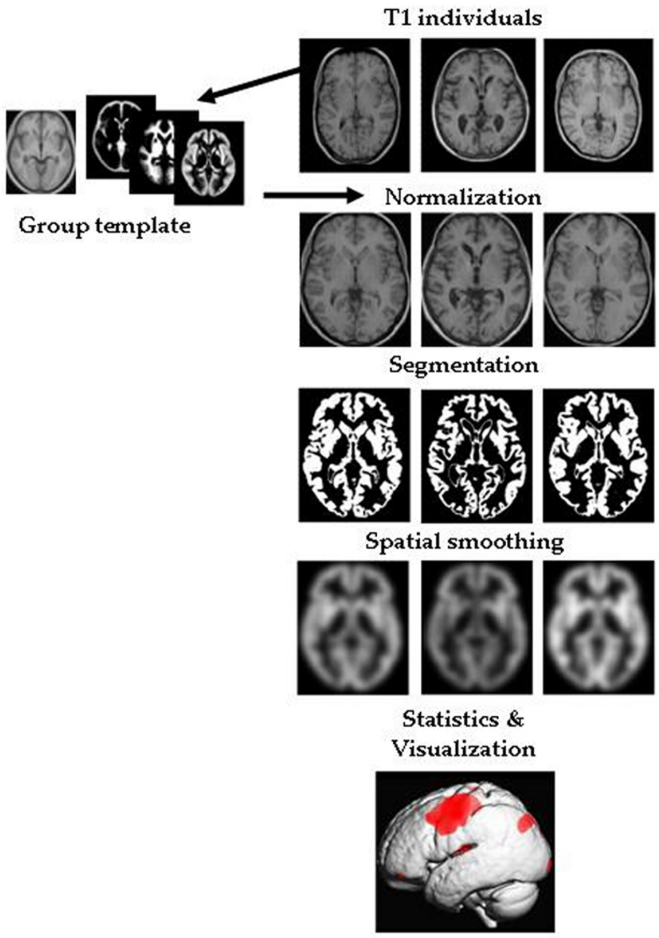

Figure 1. The primary steps of voxel-based morphometry (VBM).

4.4.4 Cortical thickness analysis (Study II)

Cortical thickness (CTH) analysis was conducted using the pipelining method developed at the McConnell Brain Imaging Centre, Montreal Neurological Institute, McGill University, Montreal, Canada (http://www2.bic.mni.mcgill.ca/). All subjects' T1-weighted 3D images were registered to standard space using the ICBM 152 template (Mazziotta *et al.* 2001) and corrected for non-uniformity artifacts (Sled *et al.* 1998). The images were then segmented into white matter (WM), gray matter (GM) and cerebrospinal fluid (CSF) using the INSECT algorithm (Zijdenbos *et al.* 2002), and the magnitude of the partial volume effect was estimated (Tohka *et al.* 2004). The brains were then automatically divided into two separate hemispheres. By using the CLASP algorithm (MacDonald *et al.* 2000, Kim *et al.* 2005), the inner and outer surfaces of the cortex were extracted according to intersections between WM and GM (white matter surface, WMS) as well as GM and CSF (gray matter surface, GMS), and the distance between the two surfaces was calculated at 40962 nodes per hemisphere with the t-link metric (Lerch *et al.* 2005a). The thickness calculations were performed on each subject's native space and then transformed back to standard space for the group analysis. The data were then smoothed with a 20 mm surface-based diffusion smoothing kernel prior to the statistical analysis (Chung *et al.* 2004). **Figure 2** illustrates the procedure of the CTH analysis.

Statistical analyses of cortical thickness were performed according to the general linear model with Matlab R2007b (MathWorks Inc., Natick, MA, USA). Significant between-group differences were tested using a t-test with a threshold of $p<0.0001$, corrected for multiple comparisons with the false discovery rate (FDR) method (Genovese *et al.* 2002). Gender and voxel size of the original image were used as nuisance variables. The correlations between clinical parameters and cortical thickness of patients with EPM1 were tested in every node by examining if the variation in cortical thickness correlated with the variation in clinical parameters.

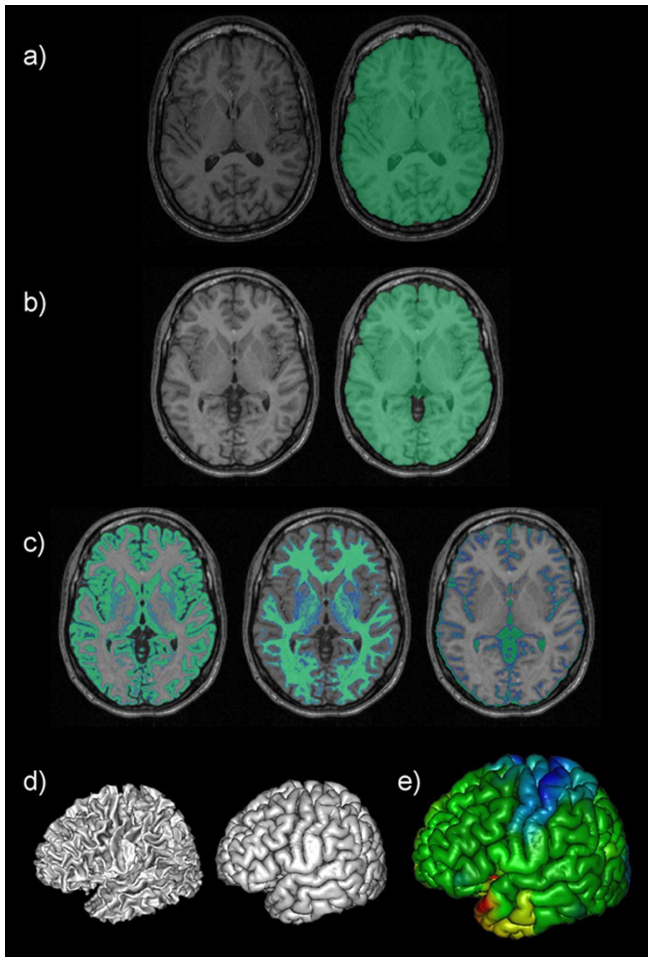

Figure 2. The procedure of cortical thickness analysis. (a) All images are registered to standard space, (b) corrected for non-uniformity artefacts and the final mask for the brain is calculated, (c) images are segmented into GM, WM and CSF, (d) inner and outer surfaces of the cortex are extracted and (e) the results are visualized.

4.4.5 Tract-based spatial statistics (Study III)

Study III was carried out in a translational research setting together with a research group studying the *Cstb* -/- mouse model of EPM1. However, the animal studies are not addressed in this thesis.

Voxelwise analysis with tract-based spatial statistics (TBSS) (Smith *et al.* 2006, Smith *et al.* 2007) was used to compare FA, axial, radial and mean diffusion (AD, RD and MD) among patients with EPM1 and controls. Prior to TBSS analysis the original data were corrected for eddy current distortions with affine (linear) alignment with FLIRT (Jenkinson *et al.* 2001, Jenkinson *et al.* 2002) which, together with all other image processing tools applied in this study, is included in the FSL software package (http://www.fmrib.ox.ac.uk/fsl/). The diffusion tensor model was calculated using the DTIFIT program and the resulting individual FA maps were used in subsequent co-registration and TBSS procedures. Direct non-linear co-registration of individual FA maps was applied to the FMRIB58 template and registration was followed by calculation of mean FA image over all subjects. The mean FA image was further thinned to represent the mean FA skeleton (white matter tracts common to all groups) **(Figure 3)**. Individual FA volumes were then projected onto this skeleton. The resulting spatially aligned FA skeleton data were finally fed to voxelwise cross-subject statistical analysis.

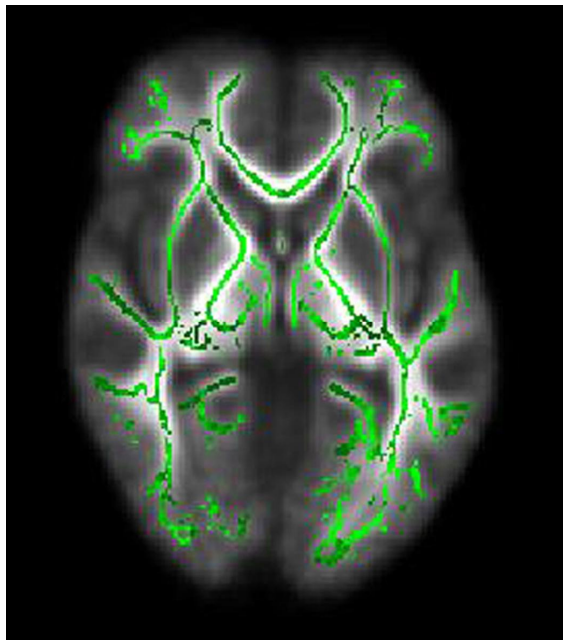

Figure 3. The mean FA skeleton displayed on the mean FA image.

Eigenvalues λ_1, λ_2, λ_3 (axial (AD), radial (RD) and mean diffusion (MD)), were brought to the same TBSS skeleton space using the co-registration warp-fields and tract projection information obtained during FA processing. For all tensor parameters null distribution in statistical testing was built up over 5000 permutations. Results are shown and reported using a threshold free cluster enhancement method (TFCE) (Smith *et al*. 2009), thresholded at a significance level $p < 0.05$.

Quantitative FA-values as well as parameters of directional diffusivity (AD, RD and MD) were extracted from regions of interest manually drawn (blinded for the significant TBSS results) along the TBSS skeleton using standard radiological definitions for white matter structures. For this purpose the mean FA TBSS skeleton was overlaid with the mean FA image to aid delineation of anatomic details. Non-midline ROIs were first drawn on the

left hemisphere and further mirrored to the right side and corrected if there was asymmetry regarding the exact positioning of the tract in question.

4.5 STATISTICS

Statistical analyses were performed with a statistical package for Windows (SPSS Inc., Chicago, IL, USA, versions 14-17). A two-tailed p value of less than 0.05 was considered significant. Normally distributed continuous-scale variables were analyzed with an independent samples t-test (Studies I-III). Nonparametric, continuous-scale data for non-normally distributed variables were analyzed with the Mann-Whitney U test (Study IV). The between group differences in VBM, cortical thickness analyses and TBSS analyses are based on t-test statistics and explained in detail in paragraphs 4.4.3, 4.4.4 and 4.4.5.

5 Results

5.1 CLINICAL FEATURES

The demographic and clinical data of EPM1 patients and controls are provided in **Table 2**. The study groups did not differ significantly with respect to age or gender. Disability of the patients with EPM1 was assessed on a three-point scale based on their Myoclonus with Action score (0-30 = mild; 31-59 = moderate; 60 or more = severe).

Table 2. Demographic and clinical data of EPM1 patients and controls

	Patients	**Controls**
Age, yr	33 ± 12 (12-64)	32 ± 10 (18-59)
Gender (M/F)	33/29	34/39
Age at onset, yr	10.2 ± 3 (5-25)	
EPM1 duration, yr	22.6 ± 10.9 (4-44)	
UMRS: Stimulus sensitivity	2.0 ± 2,3 (1-17)	
UMRS: Myoclonus with action	48.5 ± 28.7 (2-122)	
UMRS: Functional tests	9.9 ± 6.8 (1-9)	
Disability (mild/moderate/severe)*	20/21/21	

UMRS= Unified Myoclonus Rating Scale
* Grade of disability based on the Myoclonus with action score

5.2 VBM ANALYSIS OF GRAY MATTER VOLUMES (STUDY I)

Images of 34 patients and 30 controls were evaluated. Visual assessment revealed no focal signal abnormalities in the conventional images. In visual evaluation, 10 out of 34 patients had no brain atrophy, 10 out of 34 patients had mild and 13 out of 34 patients had moderate cortical atrophy within their parietal or frontal lobes, or in both. Five patients had mild atrophy of their occipital lobes. In addition, three patients had mild and two patients had moderate cerebellar atrophy. Five patients demonstrated signs of atrophy both in the cerebellum and the supratentorial structures. Two of these patients had been using phenytoin. Control individuals had no signs of brain atrophy.

VBM in patients revealed significant gray matter volume reduction in bilateral premotor and primary motor areas, supplementary motor cortex, thalami, and precuneus compared to healthy controls. The right cuneus and the left lateral orbital gyrus were also involved (**Figure 4, Table 3**). The largest significant clusters were within the motor cortex. No infratentorial changes were found. There was no GM volume reduction in healthy controls when compared to EPM1 patients.

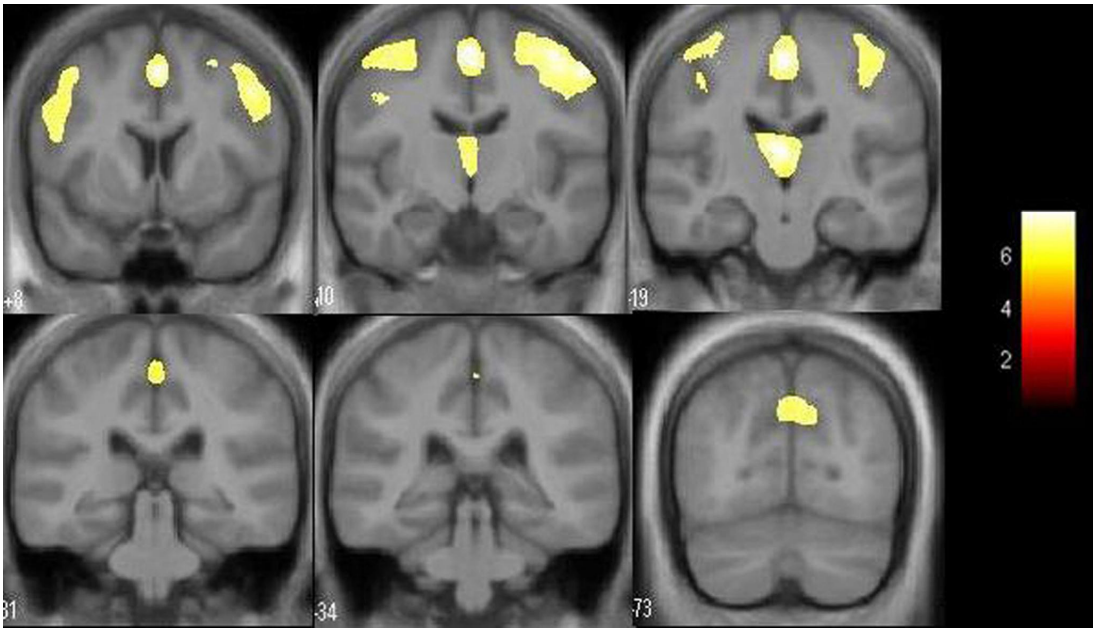

Figure 4. Areas of GM atrophy in patients with EPM1 compared with healthy controls are displayed on a study-specific mean image. VBM analysis, $p<0.05$, corrected with the FWE method. The colour bar represents T values.

When the patients were divided into two subgroups according to the duration of their disease (shorter duration ranged 6 to 10 years, n=5; longer duration ranged 11 to 41 years, n=29), no significant differences in GM volumes were found, indicating no significant progression in volume reduction.

The absolute GM volume (680.85 ± 74.32 ml), WM volume (405 ± 53.01 ml), and CSF volume (654.61 ± 116.46 ml) of EPM1 patients were all reduced compared to control subjects (GM 728.29 ± 64.94 ml, $p = 0.009$; WM 479.74 ± 45.7 ml, $p < 0.001$; CSF 744.7 ± 115.8 ml, $p = 0.003$). Accordingly, the total ICV of the EPM1 patients was smaller (1740.71 ± 216.86 ml) than the total ICV of the control subjects (1952.72 ± 191.67 ml, $p < 0.001$). There was no significant difference in the CSF/ICV ratio between patients and controls ($p = 0.47$).

Table 3. Areas of GM volume loss in EPM1 compared with controls.

Brain region	**R/L**	**MNI coordinate (x y z)**	**Cluster extent in voxels**	**T value**
Medial frontal gyrus	L	-4 6 52	8440, confluent	6.91
Superior frontal gyrus	R	3 3 53	8440, confluent	6.47
Precentral gyrus	R/L	30-10 56/-56-7 50	9688/18780	5.89/7.46
Thalamus	R/L	4-19 13/-4-17 10	6130, bilaterally confluent	7.02/6.32
Precuneus	R/L	16-94 32/-8-80 41	311/3317	5.21/7.05
Cuneus	R	17-104-7	1179	6.30
Lateral orbital gyrus	L	-40 48 -14	50	5.13

SPM random effects analysis. *P*<0,05 corrected with the family-wise error method. R=right; L=left; MNI coordinate= local maxima of each significant cluster

5.3 CORTICAL THICKNESS ANALYSIS (STUDY II)

5.3.1 Group analysis of cortical thickness

Fifty-three patients and 70 controls were evaluated. When assessed visually, there were no focal signal abnormalities in the conventional images. Statistical differences in cortical thickness between the patients with EPM1 and healthy controls at the group level are presented in detail in **Table 4 and Figure 5**. The EPM1 group displayed widespread thinning of the cortex in both hemispheres. The effects were more extensive in the left hemisphere.

Table 4. Areas of significant difference in cortical thickness between EPM1 group and controls.

Brain region	Hemisphere	Maximum t value	MNI coordinates, x,y,z
Central sulcus	right	8.83	43, -16, 36
	left	7.04	-39, -18, -45
Paracentral lobule	right	8.44	5, -26, 50
Cingulate sulcus	left	8.42	-10, -20, 46
Postcentral sulcus	left	6.93	-24, -41, 61
Superior frontal gyrus	right	7.02	6, 50, 30
Calcarine sulcus	left	9.03	-20, -70, 6
Lingual gyrus	right	6.96	5, -68, 3
Superior temporal sulcus	right	5.60	54, -15, -14
Transverse temporal gyrus	right	5.84	45, -27, 9
	left	4.48	-37, -33, 16
Middle temporal gyrus	left	5.98	-48, -66, 4
Fusiform gyrus	left	7.52	-25, -77, -9

MNI = Montreal Neurological Institute. MNI coordinates are based on a standard brain template defined by using multiple MR images of normal controls

The most significant alterations in the sensorimotor cortex were detected in the paracentral lobule bilaterally and in the depth of the central sulcus bilaterally. There was also thinning of the bilateral premotor and supplementary motor cortices and in Broca's area. The most pronounced changes in the visual cortical areas were detected bilaterally in the primary visual cortices (pericalcarine cortex). There was also thinning of the associative visual areas in the occipital lobes and the parietal associative cortex, as well as bilaterally in the temporal association cortex. Changes in the auditory areas were detected in the left primary auditory cortex. The parietal association cortex (precuneus) was bilaterally involved.

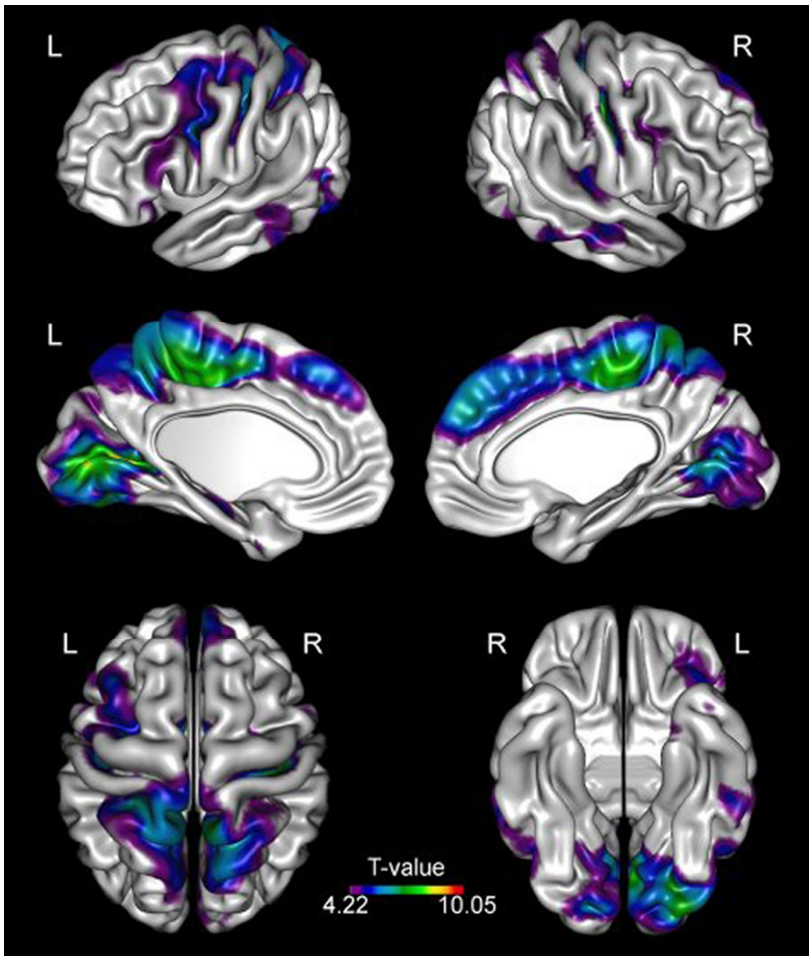

Figure 5. Group analysis of cortical thickness. Brain regions demonstrating significantly reduced cortical thickness in patients with EPM1 compared with healthy controls ($p < 0.0001$, FDR corrected).

5.3.2 CTH correlations with clinical symptoms and the duration of the disease

Figure 6 illustrates the correlation between the mean cortical thickness and age in patients with EPM1 and in controls. Cortical thickness was reduced with increasing age in both groups, but in patients, the alterations were confined to more limited areas of sensorimotor, primary and associative visual and primary auditory cortices ($p < 0.01$), whereas in controls, the age-related thinning was more diffuse throughout the hemispheres ($p < 0.01$). Furthermore, the cortex in the affected areas in EPM1 cases was thinner than in controls.

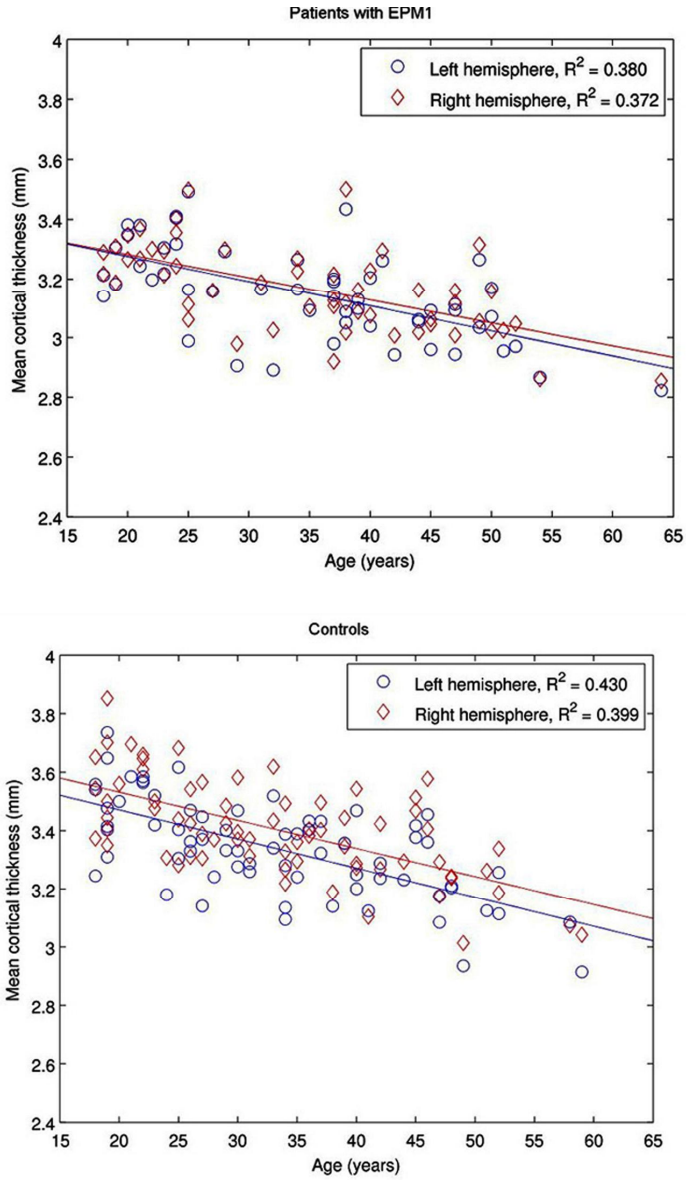

Figure 6. Scatter plots indicating correlations between age and mean cortical thickness in individual patients and controls.

In a univariate analysis there was a significant negative correlation between the duration of the disease and cortical thickness in the same regions as the age effects in EPM1 ($p < 0.01$). When age was included in the analysis as a nuisance variable, the correlations did not survive the FDR correction.

There was also a significant negative correlation between the Myoclonus with Action score and cortical thickness, especially in the pars opercularis and supramarginal gyrus bilaterally, but also in superior and inferior parietal gyri (parietal association cortex), visual areas and the premotor and prefrontal cortices bilaterally ($p < 0.05$). When illness duration was included as a nuisance variable, the correlations did not survive the FDR correction.

The correlation analysis between cortical thickness and the age at onset did not reveal any significant results.

5.4 TBSS ANALYSIS OF WHITE MATTER TRACTS (STUDY III)

Nineteen patients and 18 healthy controls were evaluated. The conventional MR images did not reveal WM abnormalities, besides a few punctate T2-hyperintensities in one patient (Fazekas grade 1) (Fazekas *et al.* 1987). Three patients had mild and nine patients had moderate cerebral atrophy. One patient had cerebellar atrophy. Seven patients had no visible brain atrophy.

TBSS revealed decreased FA values in almost all major white matter pathways in patients with EPM1 when compared with healthy controls (**Figure 7**). Global FA was decreased in EPM1 both along the TBSS skeleton (0.41 ± 0.03 vs. 0.45 ± 0.02, $p < 0.001$) and in native space (0.33 ± 0.02 vs. 0.37 ± 0.02, $p < 0.001$). Axial, radial and mean diffusion values extracted from the TBSS skeleton space followed the pattern of increased RD and MD, while AD was either unchanged or increased (**Table 5**). No statistically significant decrease was detected in AD, RD or MD in patients with EPM1.

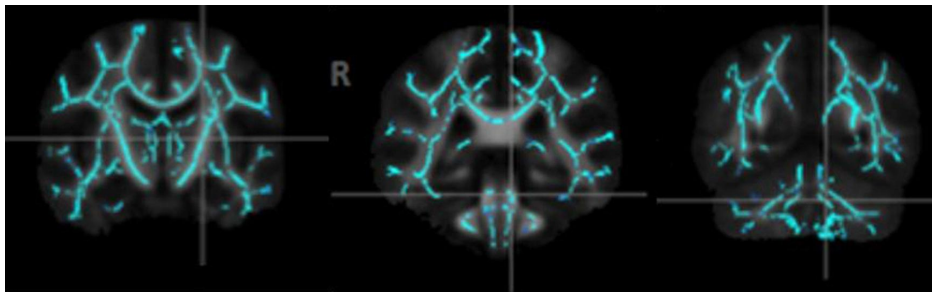

Figure 7. Decreased FA in EPM1 patients compared with controls (TFCE corrected, $p < 0.05$).

Table 5. Axial, radial and mean diffusion (x10^{-3} mm^2/s) from ROI-analysis along TBSS skeleton.

Location	Axial diffusion (x10^{-3} mm^2/s)		Radial diffusion (x10^{-3} mm^2/s)		Mean diffusion (x10^{-3} mm^2/s)		FA/AD/RD/MD
	EPM1 L/R	Control L/R	EPM1 L/R	Control L/R	EPM1 L/R	Control L/R	
Deep white matter							
Anterior limb of internal capsule	1.09 ±0.05 /1.09 ± 0.03	1.10 ± 0.07 /1.10 ± 0.07	0.51 ± 0.04 /0.51 ± 0.03	0.46 ± 0.03 /0.45 ± 0.04	0.70 ± 0.04 /0.71 ± 0.03	0.67 ± 0.04 /0.67 ± 0.04	↓, NC, ↑, ↑
Genu of internal capsule	1.22 ± 0.07 /1.23 ± 0.05	1.25 ± 0.07 /1.27 ± 0.07	0.43 ± 0.04 /0.42 ± 0.03	0.37 ± 0.03 /0.36 ± 0.03	0.69 ± 0.04 /0.69 ± 0.03	0.66 ± 0.04 /0.66 ± 0.04	↓, NC, ↑, ↑
Posterior limb of internal capsule	1.33 ± 0.07 /1.33 ± 0.07	1.34 ± 0.07 /1.34 ± 0.06	0.40 ± 0.03 /0.40 ± 0.03	0.36 ± 0.03 /0.35 ± 0.03	0.71 ± 0.03 /0.71 ± 0.04	0.69 ± 0.03 /0.68 ± 0.03	↓, NC, ↑, ↑
Genu of CC	1.51 ± 0.13	1.48 ± 0.15	0.31 ± 0.08	0.22 ± 0.06	0.71 ± 0.07	0.64 ± 0.07	↓, NC, ↑, ↑
Body of CC	1.56 ± 0.11	1.55 ± 0.10	0.46 ± 0.06	0.32 ± 0.05	0.83 ± 0.06	0.73 ± 0.07	↓, NC, ↑, ↑
Splenium of CC	1.56 ± 0.11	1.56 ± 0.12	0.22 ± 0.06	0.19 ± 0.08	0.67 ± 0.05	0.64 ± 0.07	NC, NC, NC, NC
Cingulum	1.22 ± 0.07 /1.16 ± 0.05	1.19 ± 0.07 /1.18 ± 0.06	0.47 ± 0.04 /0.51 ± 0.03	0.40 ± 0.03 /0.43 ± 0.04	0.71 ± 0.05 /0.73 ± 0.03	0.67 ± 0.03 /0.68 ± 0.04	↓, NC, ↑, ↑
IFOF/ILF	1.27 ± 0.07 /1.24 ± 0.06	1.28 ± 0.05 /1.27 ± 0.07	0.59 ± 0.05 /0.57 ± 0.05	0.51 ± 0.04 /0.50 ± 0.03	0.82 ± 0.05 /0.79 ± 0.05	0.77 ± 0.04 /0.76 ± 0.03	↓, NC, ↑, ↑
ATR/IFOF	1.01 ± 0.06 /1.02 ± 0.05	0.93 ± 0.08 /0.96 ± 0.08	0.63 ± 0.05 /0.61 ± 0.04	0.55 ± 0.05 /0.55 ± 0.05	0.76 ± 0.05 /0.75 ± 0.04	0.68 ± 0.06 /0.68 ± 0.06	↓, ↑, ↑, ↑
Thalamic white matter	1.10 ± 0.05 /1.12 ± 0.07	1.06 ± 0.05 /1.06 ± 0.05	0.63 ± 0.03 /0.66 ± 0.05	0.57 ± 0.04 /0.57 ± 0.04	0.79 ± 0.03 /0.82 ± 0.06	0.73 ± 0.04 /0.74 ± 0.04	↓, ↑, ↑, ↑

(continued)

Table 5 (continued)

Cerebellar white matter							
Sup. cerebellar white matter	0.91 ± 0.05 /0.90 ± 0.04	0.89 ± 0.04 /0.88 ± 0.04	0.64 ± 0.03 /0.63 ± 0.03	0.60 ± 0.04 /0.59 ± 0.04	0.73 ± 0.04 /0.72 ± 0.03	0.70 ± 0.04 /0.69 ± 0.03	↓, NC, ↑, ↑
Med. cerebellar white matter	0.88 ± 0.07 /0.87 ± 0.06	0.87 ± 0.05 /0.86 ± 0.05	0.60 ± 0.05 /0.58 ± 0.04	0.56 ± 0.04 /0.54 ± 0.03	0.69 ± 0.05 /0.68 ± 0.05	0.66 ± 0.04 /0.65 ± 0.04	↓, NC, ↑, ↑
Inf. cerebellar white matter	0.91 ± 0.05 /0.90 ± 0.04	0.88 ± 0.04 /0.87 ± 0.04	0.61 ± 0.04 /0.61 ± 0.04	0.56 ± 0.03 /0.56 ± 0.03	0.71 ± 0.04 /0.70 ± 0.04	0.66 ± 0.03 /0.67 ± 0.03	↓, ↑, ↑, ↑

Direction of change for each separate DTI parameter is provided either with increase (↑) or decrease (↓) in EPM1 patients relative to control group, NC = No Change. All data are mean ± SD. CC, corpus callosum. IFO, inferior fronto-occipital fasciculus. ILF, inferior longitudinal fasciculus. ATR, anterior thalamic radiation.

5.5 GENOTYPE-PHENOTYPE CORRELATIONS (STUDY IV)

5.5.1 Course of the disease

Three male and two female patients heterozygous for the dodecamer expansion and c.202C>T mutations participated in the study. Patients 1 and 2 were siblings as well as patients 3 and 4. **Table 6** presents the demographic characteristics and antiepileptic drug (AED) treatment of the patients at the time of the study visit. The age of onset of the symptoms in patients carrying the compound heterozygous mutation was found to be significantly lower than in the control EPM1 group of patients carrying homozygous mutation (7 ± 2 years vs. 10 ± 1 years, respectively, $p = 0.005$, Table 6).

5.5.2 Clinical and neurophysiological evaluation

With respect to the duration of the disease, both groups were rather homogenous (mean duration 18 ± 8 years in compound heterozygotes vs. 15 ± 8 years in homozygotes, Table 6). However, there was a significant difference in myoclonus severity between the compound heterozygous and the homozygous EPM1 patients assessed using the UMRS Myoclonus with Action score (67 ± 32 vs. 33 ± 17, $p = 0.006$, **Table 7**).

Patients 1 and 2 had limited walking ability and were wheelchair bound occasionally during severe disease episodes. An especially handicapping symptom observed with patient 1 was attacks of negative myoclonus, which in combination with strong generalized or multifocal myoclonic jerks often resulted in falls during walking. Patients 3 and 4 were completely wheelchair bound. Moreover, patient 4 had continuous spontaneous and/or movement or stimulus induced multifocal and generalized myoclonic jerks, which significantly complicated the evaluation of neurological status and UMRS scoring. The youngest female patient had the shortest duration of the disease and moderate myoclonus. The most pronounced neurological finding in this patient was ataxia. Only patient 3 was seizure-free; the remaining four patients reported 1-4 tonic-clonic seizures in 1-2 month periods despite extensive medical treatment (Table 6). All patients were dependent on the help of others in their daily life.

The available EEG data were re-evaluated based on reports, and when possible on original digital EEG recordings. There were 3 to 10 EEGs for each patient (routine, ambulatory long-term, video-EEG, or EEG-monitoring at Intensive Care Units). None exhibited a normal EEG in any of the recordings. The background activity was disturbed in all five patients, with mild slowing in one, and moderate in four. The spontaneous epileptiform activity presented as generalized irregular polyspike- or spike-wave discharges in all patients. Focal epileptiform abnormalities were also seen in all, in fronto-central regions in four, and in the occipital region of one patient. EEG and clinical photosensitivity up to clinical myoclonus or generalized seizures during photic stimulation were documented in all, and one patient also showed enhancement of occipital epileptiform abnormalities upon exogenous sensory stimuli. There was only a loose electro-clinical correlation between EEG discharges and clinical myoclonus: the clinical myoclonus was frequently reported to also occur without any simultaneous EEG correlates. Two patients had suffered from status epilepticus (SE). One initially had an EEG-confirmed generalized myoclonic status, and later, when this was resolved, exhibited a clear focal seizure with right fronto-central onset. The other SE patient suffered from clinically convulsive SE, but the EEG was recorded when the patient was already sedated under propofol.

Table 6. Demographic data, seizure frequency and treatment at the study visit.

Patient Nr	**Gender**	**Age**	**Age at symptom onset**	**EPM1 duration**	**Tonic-clonic seizure frequency**	**Treatment at study visit (mg/d)**	**Expansion length (allele 1/allele 2)**
1	M	23	5	18	1-2 per month	VPA 2100; LTG 200; LEV 2250; PIR 31200	2/71
2	M	21	7	14	1 per 2-3 month	VPA 1100; LTG 200; LEV 2000	2/70
3	F	34	10	24	Seizure-free	VPA 900; CZP 2.25; TPM 125; PIR 2400	2/61
4	M	37	7	29	1-2 per month	VPA 1200; CZP 4; LEV 1500; PIR 3600	2/61
5	F	14	6	8	2-4 per month	VPA 1400; CZP 6	2/70
Compound heterozygote group[a]	3M/2F	26 ±9 (14-36)	7 ± 2 (5-10)	18 ± 8 (8-29)	---	---	2/67 ± 5 (61-71)
Expansion homozygote group[a]	11M/10F	25 ±9 (12-38)	10 ± 1 (7-12)	15 ± 8 (4-28)	---	---	64 ±5 (55-73) / 68 ±4 (60-75)

M, Male; F, Female; VPA, valproate; LTG, lamotrigine; LEV, levetiracetam; PIR, piracetam; CZP, clonazepam; TPM, topiramate. [a] Data presented as Mean ± St. Dev (Minimum-Maximum) unless otherwise indicated

.

Table 7. Disease status and UMRS test scores of EPM1 patients at the study visit.

Patient Nr	Walking ability	UMRS: patient questionnaire score	UMRS: stimulus sensitivity score	UMRS: myoclonus with action score	UMRS: functional test score
1	Assisted walking, wheelchair regularly	19	1	56	8
2	Able to walk, wheelchair occasionally	4	1	50	5
3	Wheelchair bound	22	2	69	9
4	Wheelchair bound	33	13	122	22
5	Able to walk	12	0	40	8
Compound heterozygote group[a]	1/2/2[b]	18 ± 11 (4-33)	4 ± 5 (0-13)	67 ± 32 (40-122)	10 ± 7 (5-22)
Expansion homozygote group[a]	19/1/1[b]	7 ± 6 (0-17)	1 ± 2 (0-8)	33 ± 17 (12-84)	7 ± 4 (1-17)

[a] Data presented as Mean ± St. Dev (Minimum-Maximum) unless otherwise indicated
[b] Able to walk/Occasional wheelchair use/Wheelchair bound
UMRS, Unified Myoclonus Rating Scale

5.5.3 Neuropsychology

The intellectual performance of the compound heterozygous patients was below the normal range and the cognitive dysfunction of individual patients in verbal and performance tasks varied from mild to severe. Two of the youngest patients (1 and 5) had severe cognitive impairment and have needed special schooling. Patient 2 had only mild cognitive impairment but needed special vocational rehabilitation after normal school. Patients 3 and 4 developed moderate cognitive impairment after finishing normal school. Patients 1-4 are now receiving disability pension; patient 5 is still at school.

As a group these patients had a lower mean VIQ and PIQ than the control EPM1 patients (VIQ 75 ± 10 vs. 90 ± 14, $p = 0.044$; PIQ 57 ± 13 vs. 79 ± 15, $p = 0.013$). In the learning of the word list, the two groups performed similarly, but the compound heterozygous patients had poorer immediate recall of the stories. In delayed memory measures the groups did not differ. In the visuomotor task the performance of the compound heterozygous patients was significantly impaired compared with the control EPM1 group.

5.5.4 MR imaging

Visual assessment of conventional images revealed mild frontotemporal post-traumatic changes in patient 4 but the other patients had no focal abnormalities. In addition, patient 4 had moderate cerebellar and mild cerebral atrophy. Patient 3 had moderate cerebellar atrophy and patient 1 had moderate cerebral atrophy. Patients 2 and 5 had no visible brain atrophy. In the control EPM1 group of 21 patients who are homozygous for the major mutation, six patients had mild or moderate cerebral atrophy, one patient had mild cerebellar atrophy and three patients had mild or moderate cerebral and cerebellar atrophy. The remaining eleven patients had no visible brain atrophy.

An ROI-based VBM analysis of the primary motor and premotor cortex, supplementary motor cortex and thalami revealed GM volume loss in all of those areas when compared with the 24 healthy controls (**Figure 8**). There were no significant GM volume changes between the homozygous and the compound heterozygous patients. DTI and MRS could be performed only on patient 3 of the compound heterozygote group, and thus no statistical comparisons were feasible. In MRS the lactate concentration was increased in the CSF of patient 3.

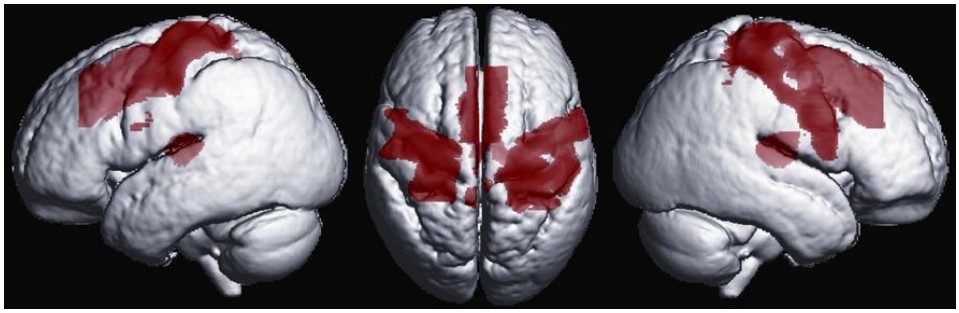

Figure 8. Areas of gray matter atrophy in compound heterozygous EPM1 patients compared with controls superimposed on a volume rendered average image of the study population. VBM analysis, $p<0.02$ corrected with the FDR method.

6 Discussion

In the present study, the MR imaging findings of patients with EPM1 have been compared with those of healthy controls in order to explore whether modern imaging techniques would reveal previously undetected structural changes in the brains of the patients. Furthermore, the phenotype-genotype correlations between two groups of patients with different mutations in *CSTB* have been addressed. The high prevalence of EPM1 in Finland offered a unique opportunity to evaluate, at present, the largest number of patients with EPM1 at the same study center.

6.1 GRAY MATTER VOLUME LOSS IN EPM1 (STUDY I)

In the present study of 34 patients with EPM1, VBM revealed significant volume loss in supratentorial gray matter, particularly within the cortical motor areas. Thalami and precunei were also affected bilaterally. When assessed visually, mild to moderate cerebral atrophy was present in most of the patients, but any regional changes in gray matter volume were too subtle to detect.

According to the VBM analysis, no infratentorial changes were found in the group comparison with healthy controls. Previously, volume loss of the structures in the posterior fossa has been reported, along with unspecific cortical atrophy (Mascalchi *et al.* 2002). The neuropathological findings in the animal model of EPM1, the *Cstb* -/- mice, consist of severe loss of cerebellar granule cells due to apoptotic cell death; less marked neuronal apoptosis in the hippocampal formation and entorhinal cortex in younger animals; and gliosis in the hippocampal formation, entorhinal cortex, neocortex, and striatum in older animals (Pennacchio *et al.* 1998, Shannon *et al.* 2002). These data from both human and animal studies suggest that changes in the posterior fossa structures play a major role in the pathophysiology of EPM1. However, in the group analysis we found no infratentorial changes. In visual evaluation mild or moderate cerebellar atrophy was detected in only five of 34 patients. Two of these patients had been using phenytoin in the past (Eldridge *et al.* 1983), and one patient had a history of excessive alcohol use. These factors may have contributed to the development of cerebellar atrophy. In the previous study reporting atrophy in the posterior fossa (Mascalchi *et al.* 2002), the number of patients is substantially smaller than in the present study, which may also explain the discrepancy between the results. In view of the results of Study I, it seems that in patients the supratentorial changes may be a significant pathophysiological factor. However, although VBM failed to demonstrate pathology in the posterior fossa, DTI of the same patients did reveal changes in the cerebellum, thus adding to the results of the study.

The mechanism that causes the observed gray matter volume loss in cortical motor areas and thalami remains unknown, as the overall pathophysiology of EPM1 is still poorly understood. The clinical myoclonus in EPM1 is considered epileptic (i.e., cortical) in nature (Caviness *et al.* 2004). Advanced electrophysiological methods such as magnetoencephalography (MEG), somatosensory evoked fields (SEF), EEG, somatosensory evoked potentials (SEP), and long-loop reflexes have been applied to EPM1 patients (Canafoglia *et al.* 2004, Forss *et al.* 2001, Silen *et al.* 2000, Silen *et al.* 2002a, Silen *et al.* 2002b, Visani *et al.* 2006). These studies have provided indirect evidence of increased cortical inhibition and disturbed activation, as well as hyperexcitability of the sensorimotor cortex. Transcranial magnetic stimulation (TMS) is particularly well suited to study the inhibitory/excitatory balance of the motor cortex. A recent study of 24 patients with EPM1

suggests a prevailing inhibitory tonus of the primary motor cortex as a possible reactive mechanism to the disease (Danner *et al.* 2009). Earlier, evoked potential studies have also shown abnormalities beyond the primary motor cortex in the thalamocortical loops (Mervaala *et al.* 1984, Mervaala *et al.* 1986), and a recent PET study also points to a thalamocortical dopaminergic defect in EPM1 (Korja *et al.* 2007b).

The total intracranial volume of the EPM1 patients was smaller than that of healthy controls but the CSF/ICV ratio was not reduced compared to controls, indicating that there was no general brain atrophy in EPM1 patients. This might suggest that EPM1 patients have a smaller head size than healthy controls. However, a previous study of 93 Finnish EPM1 patients reports normal head circumferences (Koskiniemi *et al.* 1974a). Thickening of the skull has also been observed (Koskiniemi *et al.* 1974a, Korja *et al.* 2007a), but skeletal changes in EPM1 are not addressed in this thesis.

In a retrospective study on long-term evolution of Unverricht-Lundborg disease in 20 patients who had been closely followed since the onset of their disease symptoms, myoclonus progressed only during the first 5 years of apparent disease (Magaudda *et al.* 2006). These results indicated that EPM1 progresses over a limited period and stabilizes thereafter, and the authors speculated that the self-limited progression might be the consequence of age-related apoptosis in selected neuronal populations. When we divided our patient population into those with a shorter (range 6-10 years) or longer (range 11-41 years) duration of the disease since diagnosis, and compared their gray matter volume loss with VBM, we observed no significant difference. This may reflect the phenomenon described in the aforementioned study (Magaudda *et al.* 2006). However, to reliably correlate the VBM findings with the clinical severity of the disease, a larger patient population would be necessary.

A limitation of Study I is that the VBM analysis concentrates on the volumes of gray matter structures but it is considered to be less reliable in analyses of white matter. The results of the present study indicate that the disease affects the cortical gray matter in the motor areas. While the mechanism of this finding remains to be verified, a more detailed comparative analysis of the pyramidal tract structures with the use of diffusion tensor imaging and detailed neurophysiological evaluation will be warranted in the future.

6.2 REGIONAL CHANGES IN CORTICAL THICKNESS OF PATIENTS WITH EPM1 (STUDY II)

The myoclonic jerks in EPM1 are often provoked by a variety of exogenic stimuli (Kälviäinen *et al.* 2008, Koskiniemi *et al.* 1974a); however, morphological changes in the sensory cortical areas of the brain have not been reported. In addition, there is considerable variation in the severity of the disease between patients and even within the same family (Kälviäinen *et al.* 2008), but to the best of our knowledge, no correlations between quantitative structural changes in the brain and clinical parameters such as the duration of the disease, age at onset or myoclonus severity have been investigated so far.

In agreement with the VBM findings, significant and progressive thinning of the cortical motor areas of patients with EPM1 was found in comparison to the healthy controls. This type of thinning of the motor cortex has not been reported previously, and it may be related to the most disabling symptoms in EPM1, i.e. myoclonus. In previous MEG studies the origin of cortical myoclonus has been localized to the sensorimotor cortex (Mima *et al.* 1998a, Mima *et al.* 1998b).

As a novel finding, we found extensive changes in the cortical sensory areas, the visual areas and the auditory areas as well. Cortical thinning in the sensory areas extended well beyond the primary and secondary somatosensory, visual and auditory cortices. For instance, the parietal association cortex was extensively affected. This area is involved in

important cortical functions, e.g. visual localization of objects, elaboration of motor program necessary to reach these objects, spatial perception and spatial memory in collaboration with the visual association cortex, and auditory functions especially in the supramarginal gyrus in conjunction with the auditory association cortex (Mesulam 1998). The areas of regionally reduced cortical thickness were in parallel with the severity of the action myoclonic symptoms of EPM1. Alterations in the visual and auditory cortices thus seem to be congruent with the stimulus-sensitive nature of the symptoms. Interestingly, cortical thinning was also observed in the Broca's area, but the relevance of this finding remains to be clarified.

TMS (Canafoglia *et al.* 2004, Danner *et al.* 2009) and MEG (Silen *et al.* 2000) studies have pointed to impaired sensorimotor cortical inhibition in EPM1. An absence of activation of the secondary sensory cortex (SII) has been reported in patients who exhibited more severe motor symptoms (Forss *et al.* 2001), and the authors speculated that deficient activation of SII could account for the disturbed sensorimotor integration, contributing to impaired movement coordination. The same phenomenon may be reflected in our finding that the Myoclonus with Action score correlated negatively with cortical thickness in the sensory areas, including the SII area. Patients with more severe myoclonus had thinner sensorimotor cortical areas than patients with milder symptoms.

The duration of the disease correlated negatively with cortical thickness in our univariate analysis. However, one cannot be absolutely certain that the process of cortical thinning in EPM1 is progressive. Since all the clinical parameters we have evaluated seem to correlate with each other as well as cortical thickness, it is difficult to totally separate their effects. Age correlated negatively with cortical thickness both in patients and controls, but in patients, the findings were more limited. Thus the progression of cortical thinning cannot be explained by age alone. The affected cortical areas seemed to be thinner in EPM1 cases than in controls, even in young individuals. The onset of EPM1 is in early childhood or late adolescence, the peak being around 12-13 years (Genton 2010), and before the onset of symptoms the disease process has probably already had an effect on the brain. This may explain the more limited age related thinning of cortex in patients with EPM1.

In the control group the effects of aging were consistent with previous reports of age affecting the prefrontal and parietal cortices negatively, as well as gray matter around the central sulcus and the relative sparing of temporal and parahippocampal cortex (Salat *et al.* 2004, Thambisetty *et al.* 2010). Other investigations have also found that the occipital lobes, and particularly the visual cortex, are negatively affected by age (Salat *et al.* 2004, Gaetz *et al.* 2011). In a study of normal aging with 883 participants the results were fairly similar to those in our study (Fjell *et al.* 2009). In the present study the pericalcarine cortex was relatively spared in healthy controls, but interestingly, it was more extensively affected in EPM1 cases. The mean age of the control group in our study was 33 years, which is substantially younger than in previous reports, and this might explain some of the differences in the results.

There was some variation in the slice thickness (1 to 1.2 mm) of the MR images, which is a limitation in Study II. However, from 123 scans in only 16 did the slice thicknesses differ from 1 mm, and slice thickness was also included as a nuisance variable in the statistical analyses. Therefore it should not affect the results significantly. Cortical thickness analysis concentrates on the cerebral cortex and cannot be applied to deep gray matter, cerebellum or white matter, which can thus be considered as another limitation of the method. In the future, it may be possible to gather more information on the subcortical pathways by utilizing diffusion tensor imaging together with cortical thickness analysis.

6.3 WHITE MATTER CHANGES IN EPM1

Study III aimed to clarify the possible changes in the white matter tracts of patients with EPM1 by applying diffusion tensor imaging with TBSS analysis. TBSS revealed decreased FA in the pyramidal tracts of patients with EPM1. However, the changes in WM extended far beyond the corticospinal tracts. FA was also decreased in thalamic WM, the corpus callosum and in the association fibers as well. There were also significant changes in the cerebellar WM.

Previous studies have revealed loss of neuronal volume in the structures of the posterior fossa (Mascalchi *et al.* 2002), in agreement with the observed GM volume loss particularly in the cortical motor areas and thalami (Study I), and thinning of the sensorimotor cortex (Study II). T2 hyperintensities in the basal ganglia and WM of EPM1 patients have also been reported (Korja *et al.* 2010). The finding of motor cortex abnormalities is in agreement with the results of a navigated TMS study, suggesting an impairment of cortical inhibitory networks (Danner *et al.* 2009). Earlier studies with evoked potentials have also reported abnormalities beyond the primary motor cortex in the thalamocortical loops (Mervaala *et al.* 1984, Mervaala *et al.* 1986). Furthermore, it has been speculated that the cerebellum may modulate the balance between inhibition and facilitation in the motor cortex, and that cerebellar pathology may play a role in the mechanisms involved in provoking action myoclonus (Tijssen *et al.* 2000). In view of the results of the present study, it seems that both supratentorial and cerebellar changes are major factors contributing to the pathophysiology of EPM1.

To evaluate the changes in the WM in more detail, we analyzed other diffusivity parameters (AD, RD and MD). The alterations in the diffusivity parameters in the majority of the examined supratentorial ROIs follow the pattern of chronic WM degeneration (FA decrease, increase in RD and MD) as reported in a recent study of age-related differences in white matter (Burzynska *et al.* 2010). This pattern is thought to reflect axonal and myelin loss (Concha *et al.* 2006, Sun *et al.* 2008).

The histopathological data of EPM1 is limited. The data from patients consists of diffuse loss of cerebellar granule and Purkinje cells, degeneration and loss of neurons in the cerebral cortex, striatum, thalamus, brainstem nuclei and in spinal motor neurons (Eldridge *et al.* 1983, Koskiniemi *et al.* 1974a, Haltia *et al.* 1969). In animal studies with *Cstb*-deficient mice, severe loss of cerebellar granule cells has been found (Pennacchio *et al.* 1998). In younger animals there was less marked neuronal apoptosis in the hippocampal formation and entorhinal cortex. Gliosis in the hippocampal formation, entorhinal cortex, neocortex and the striatum was present in older animals. There was also widespread gliosis of the WM (Shannon *et al.* 2002).

The extensive changes in the subcortical WM, pyramidal tracts, thalami and cerebellar WM of patients with EPM1 parallel the previous imaging reports and the sparse histopathology data of EPM1. However, the mechanism of the WM degeneration remains yet to be clarified. It is also unclear whether the GM changes are secondary to the WM degeneration, or vice versa.

6.4 PHENOTYPE OF EPM1 IN COMPOUND HETEROZYGOUS PATIENTS

EPM1 follows autosomal recessive inheritance and is caused by mutations of the cystatin B (*CSTB*) gene (Pennacchio *et al.* 1996). Most patients are homozygous for the expanded dodecamer repeat mutation alleles, but eleven other EPM1-associated mutations have also been identified (Joensuu *et al.* 2008, Lalioti *et al.* 1997b, Erdinc *et al.* 2010). With the exception of the missense p.Gly4Arg mutation (Lalioti *et al.* 1997a), these other mutations have been reported to occur in compound heterozygosity with the expansion mutation. In

study IV, the clinical, cognitive and imaging characteristics of five EPM1 patients who are compound heterozygous for the dodecamer repeat expansion and the c.202C>T mutations were evaluated.

In visual evaluation, one of the compound heterozygous patients had signs of brain contusion in the MR images, which is not surprising considering the myoclonic jerks that can be severe enough to cause a person to fall down. VBM findings of the compound heterozygous patients did not differ from those of the patients homozygous for the expansion mutation. When we performed a VBM analysis between the compound heterozygous EPM1 patients and healthy controls, based on the brain areas that were found to be atrophic in EPM1 patients carrying the homozygous mutation, the most significant clusters of GM volume loss were in the supplementary motor cortex. There was also GM volume loss in the primary and premotor cortex and the thalamus bilaterally. It is possible that there are no structural differences between the two genotypes. On the other hand, the number of compound heterozygous patients in the present study was quite small and thus any subtle differences may be difficult to detect. In a recent TMS study, the same patients exhibited functional changes in primary motor cortical areas, congruent with their structural changes (Danner *et al.* 2011).

In spectroscopy, an increase in lactate concentration was observed in the CSF of patient 3, suggesting that cerebral energy metabolism may be affected in EPM1 through a yet unidentified mechanism. However, this finding needs further investigation with data from more subjects. We could not perform MRS for the rest of the compound heterozygous patients due to myoclonic jerks which made it impossible to continue scanning for a sufficient time. For the same reason DTI was feasible in only one patient. MR imaging of patients with this particular mutation in the *CSTB* gene seems to be more challenging than imaging patients with the major mutation.

It has been believed that similar disease manifestation develops in patients with EPM1 irrespective of the underlying mutations. Previous studies characterizing EPM1 patients have found no genotype-phenotype correlations, including no association between the length of the expanded dodecamer repeat and the age of onset of the disease or its severity (Virtaneva *et al.* 1997, Lalioti *et al.* 1998). However, the results of Study IV show that compound heterozygosity for the dodecamer expansion and the c.202C>T mutation in the *CSTB* gene is associated with earlier onset of symptoms. Moreover, the patients carrying such a mutation are more likely to have a more severe form of the disease, resulting in more severe myoclonus and treatment-resistant epileptic seizures. It has previously been reported that in EPM1, the epileptic seizures have a positive response to AED treatment (Iivanainen *et al.* 1982) and tend to decrease in frequency or cease completely within 10-15 years from the onset of the disease (Norio *et al.* 1979, Magaudda *et al.* 2006). In the present study, three of the compound heterozygous patients, with a disease duration of over 10 years, were still suffering from tonic-clonic seizures despite extensive AED treatment. Therefore it seems that epileptic seizures in EPM1 patients that are compound heterozygous for the dodecamer expansion mutation and the c.202C>T mutation are more drug-resistant than in EPM1 cases caused by the homozygous expansion mutation. The myoclonus in compound heterozygous patients also seems to be more severe and incapacitating and it seems to lead to earlier and more frequent use of a wheelchair as compared with homozygous patients.

Instability of the c.202C>T mutant transcript and protein has been suggested based on real-time quantitative PCR and Western analyses in patients' cells and through *in vitro* transfection experiments (Alakurtti *et al.* 2005, Joensuu *et al.* 2007). Therefore, the more severe clinical manifestations in the compound heterozygous patients are likely to reflect the reduced amounts of the CSTB protein in the patients' cells compared to the cells of

patients homozygous for the expansion mutation, rather than a dominant negative effect of the mutant p.Arg68X transcript.

Scalp EEGs showed, in addition to generalized epileptiform discharges more focal / regional epileptiform activity over fronto-centro-temporal regions in all patients. These spikes or sharp waves occurred separately, in trains, or as electrographic seizures of 13 seconds or less. EEG in EPM1 usually shows features of generalized epilepsy (Shahwan *et al.* 2005), whereas focal epileptiform abnormalities have not been previously described (Kälviäinen *et al.* 2008). Interestingly, these focal features were seen over sensory-motor head regions, where the structural changes were found.

The cognitive intellectual performance of compound heterozygous patients seems to be poorer than that of homozygous patients, especially in regards to performance tasks and with visuomotor skills. The compound heterozygous patients seem to need special education because of their cognitive problems, whereas this is not the case in homozygous patients, who usually perform normally in school and may have their vocational education and employment limited more by their motor symptoms.

The current study shows that the patients carrying compound heterozygous dodecamer repeat expansion and c.202C>T mutations in the *CSTB* gene seem to have a more severe form of EPM1 than the patients who are homozygous for the expansion mutation. Even though the number of compound heterozygous patients in Study IV was quite small, it has nevertheless been shown that the type of genetic mutation does indeed play a role in the disease phenotype, which has implications for the counseling of patients.

6.5 LIMITATIONS OF THE STUDY

As the myoclonic symptoms in EPM1 are stimulus-sensitive, the loud noise of the MR scanner can cause problems during imaging. The possibility of motion artifacts has to be considered. Motion correction software is nowadays available in clinical scanners; however, it cannot be utilized with the T1-3D sequences needed for VBM or cortical thickness analysis. Particularly the compound heterozygous patients in the present study seemed to be quite sensitive to the noise of the scanner, and DTI for example was feasible with only one of them. Spectroscopy was also challenging for the compound heterozygotes due to the long scanning time, although the sequence itself is not that noisy. Nevertheless, in most cases the image quality was good. It is helpful to keep the atmosphere during scanning as calm as possible and to use proper hearing protection to reduce the noise.

The patient populations in Studies III and IV were quite small. During the time when the imaging data were acquired, the software in the MR scanner used in the present study was upgraded, and the DTI sequence changed. Thus only 19 patients were imaged with the same sequence and could be included in Study III. As for Study IV, we aimed to evaluate different genotypes in EPM1, and at present there are only five known patients in Finland who are compound heterozygous for the dodecamer expansion mutation and the c.202C>T mutation.

The slice thickness of the T1-3D images varied between 1.0 mm to 1.2 mm depending on the size of the head, but the in-slice resolution was 1.0 mm x 1.0 mm. In the majority of the cases the slice thickness was, however, 1.0 mm and the issue has been taken into account in the statistical analyses. Therefore it is not likely that slice thickness variation has affected the results significantly.

The methods used in the present study are based on group comparisons. Thus they cannot be applied to the analysis of individual patients. Furthermore, this is a cross-sectional study, and prospective studies with advanced imaging would be needed to gain more conclusive data on the possible progression of structural changes in the brains of patients with EPM1.

6.6 FUTURE CONSIDERATIONS

Sophisticated MRI techniques and new analysis methods enable group comparisons and reveal subtle morphological changes that cannot be detected by visual inspection of individual cases. In addition, group analyses provide an opportunity to correlate clinical parameters such as neuropsychological results with the structural alterations discovered with imaging.

The combination of various MRI techniques offers complementary information about the pathophysiology of EPM1. For example, in the present study DTI brought out cerebellar alterations in addition to changes in the supratentorial WM, while VBM and cortical thickness analysis disclosed changes in the supratentorial GM structures.

Although advanced MR imaging has revealed previously undiscovered morphological changes in the brains of patients with EPM1, the molecular and histopathological pathogenesis of EPM1 still remains to be elucidated. The results of the present work may help in future studies that aim to clarify the cellular mechanisms that result in the phenotype of EPM1. By correlating the imaging findings in humans with those of *Cstb*-deficient mice and focusing on the possible structural changes common to both, it may be possible to gain more histopathological information about EPM1.

Transcranial magnetic stimulation is considered to be particularly well suited to study the inhibitory/excitatory balance of the motor cortex. Future TMS studies guided by the data from structural MRI studies would likely add to the current knowledge of the pathogenesis of EPM1. It is likely that the brain's functional responses to various stimuli are also altered in EPM1. With fMRI it would be possible to study the activation of different cortical areas, and by combining the results with those of neurophysiological studies a more comprehensive picture of the pathophysiology may be accomplished. Furthermore, evaluation of the possible changes in brain metabolism of patients with EPM1 by utilizing MR spectroscopy would be important and might give further insight to the pathogenesis of EPM1.

Finally, the advanced neuroimaging methods used here may also be useful in studying other neurodegenerative disorders. It would be valuable to see whether there are similar structural changes in other conditions with movement disorders, or if the alterations found in the present study are specific to EPM1.

7 Conclusions

1. Patients with EPM1 show significant loss of gray matter volume bilaterally in the motor cortex and thalamus, when compared with healthy controls. The atrophic changes are consistent with the motor symptoms of EPM1.

2. In cortical thickness analysis the patients with EPM1 show thinning of the sensorimotor, visual and auditory cortices in comparison with healthy controls. These cortical areas are consistent with the stimulus-sensitive nature of the symptoms of EPM1. Cortical thickness (CTH) correlates negatively with clinical parameters such as age, the duration of EPM1 and the severity of myoclonus. The effects of the clinical parameters on CTH cannot be totally separated because of their correlation with each other. The results do, however, suggest that the process of cortical thinning is progressive.

3. Patients with EPM1 exhibit extensive chronic degeneration of both supratentorial and infratentorial white matter (WM), when compared with healthy controls. Changes in the directional diffusivity parameters indicate that the WM changes may reflect axonal and myelin loss.

4. The phenotype of EPM1 seems to be more severe in patients heterozygous for the dodecamer repeat expansion and the c.202C>T mutations in the cystatin B gene, compared with patients homozygous for the dodecamer repeat expansion. The age at onset of symptoms seems to be younger. These patients also have more severe myoclonus and drug-resistant tonic-clonic seizures. Moreover, their cognitive performance is lower. These findings have implications for the counseling of EPM1 patients with different genetic findings.

5. The results of Studies I-III point to widespread neurodegenerative changes throughout the brain, explaining the poor response to AED treatment in EPM1. This should be taken into account in future studies and in the counseling of patients.

8 References

Alakurtti K, Weber E, Rinne R, Theil G, de Haan GJ, Lindhout D, Salmikangas P, Saukko P, Lahtinen U and Lehesjoki AE. Loss of lysosomal association of cystatin B proteins representing progressive myoclonus epilepsy, EPM1, mutations. Eur.J.Hum.Genet. 2005;13:208-215.

Ashburner J and Friston KJ. Voxel-based morphometry-the methods. Neuroimage 2000;11:805-821.

Ashburner J, Hutton C, Frackowiak R, Johnsrude I, Price C and Friston K. Identifying global anatomical differences: deformation-based morphometry. Hum.Brain Mapp. 1998;6:348-357.

Basser, P.J. 2009, "Diffusion and diffusion tensor MR imaging: Fundamentals" in Magnetic resonance imaging of the brain and spine, ed. S.W. Atlas, 4th edn edn, Lippincott Williams & Wilkins, a Wolters Kluwer business, Philadelphia, USA, pp. 1752-1767.

Bendel P, Koivisto T, Hänninen T, Kolehmainen A, Könönen M, Hurskainen H, Pennanen C and Vanninen R. Subarachnoid hemorrhage is followed by temporomesial volume loss: MRI volumetric study. Neurology 2006;67:575-582.

Bendel P, Koivisto T, Niskanen E, Könönen M, Äikiä M, Hänninen T, Koskenkorva P and Vanninen R. Brain atrophy and neuropsychological outcome after treatment of ruptured anterior cerebral artery aneurysms: a voxel-based morphometric study. Neuroradiology 2009;51:711-722.

Berkovic SF, Mazarib A, Walid S, Neufeld MY, Manelis J, Nevo Y, Korczyn AD, Yin J, Xiong L, Pandolfo M, Mulley JC and Wallace RH. A new clinical and molecular form of Unverricht-Lundborg disease localized by homozygosity mapping. Brain 2005;128:652-658.

Bernasconi N, Bernasconi A, Caramanos Z, Antel SB, Andermann F and Arnold DL. Mesial temporal damage in temporal lobe epilepsy: a volumetric MRI study of the hippocampus, amygdala and parahippocampal region. Brain 2003;126:462-469.

Bernhardt BC, Worsley KJ, Besson P, Concha L, Lerch JP, Evans AC and Bernasconi N. Mapping limbic network organization in temporal lobe epilepsy using morphometric correlations: insights on the relation between mesiotemporal connectivity and cortical atrophy. Neuroimage 2008;42:515-524.

Betting LE, Li LM, Lopes-Cendes I, Guerreiro MM, Guerreiro CA and Cendes F. Correlation between quantitative EEG and MRI in idiopathic generalized epilepsy. Hum.Brain Mapp. 2010;31:1327-1338.

Beyer MK, Janvin CC, Larsen JP and Aarsland D. A magnetic resonance imaging study of patients with Parkinson's disease with mild cognitive impairment and dementia using voxel-based morphometry. J.Neurol.Neurosurg.Psychiatr. 2007;78:254-9.

Brandao, L. & Domingues, R. 2004, MR spectroscopy of the brain, Lippincott Williams & Wilkins, Philadelphia, USA.

Burzynska AZ, Preuschhof C, Backman L, Nyberg L, Li SC, Lindenberger U and Heekeren HR. Age-related differences in white matter microstructure: region-specific patterns of diffusivity. Neuroimage 2010;49:2104-2112.

Canafoglia L, Ciano C, Panzica F, Scaioli V, Zucca C, Agazzi P, Visani E, Avanzini G and Franceschetti S. Sensorimotor cortex excitability in Unverricht-Lundborg disease and Lafora body disease. Neurology 2004;63:2309-2315.

Cascino GD, So EL, Buchhalter JR and Mullan BP. The current place of single photon emission computed tomography in epilepsy evaluations. Neuroimaging Clin.N.Am. 2004;14:553-561, x.

Caviness JN and Brown P. Myoclonus: current concepts and recent advances. Lancet Neurol. 2004;3:598-607.

Chew NK, Mir P, Edwards MJ, Cordivari C, Martino D, Schneider SA, Kim HT, Quinn NP and Bhatia KP. The natural history of Unverricht-Lundborg disease: a report of eight genetically proven cases. Mov.Disord. 2008;23:107-113.

Chung M and Taylor J 2004, "Diffusion smoothing on brain surface via finite element method", Proceedings of the 2004 IEEE International Symposium on Biomedical Imaging: From Nano to MacroIEEE, 15-18 April 2004, pp. 432.

Cohen NR, Hammans SR, Macpherson J and Nicoll JA. New neuropathological findings in Unverricht-Lundborg disease: neuronal intranuclear and cytoplasmic inclusions. Acta Neuropathol. 2011;121:421-427.

Concha L, Gross DW, Wheatley BM and Beaulieu C. Diffusion tensor imaging of time-dependent axonal and myelin degradation after corpus callosotomy in epilepsy patients. Neuroimage 2006;32:1090-1099.

Cousins JP. Clinical MR spectroscopy: fundamentals, current applications, and future potential. AJR Am.J.Roentgenol. 1995;164:1337-1347.

Damoiseaux JS, Smith SM, Witter MP, Sanz-Arigita EJ, Barkhof F, Scheltens P, Stam CJ, Zarei M and Rombouts SA. White matter tract integrity in aging and Alzheimer's disease. Hum.Brain Mapp. 2009;30:1051-1059.

Danner N, Julkunen P, Khyuppenen J, Hukkanen T, Könönen M, Säisänen L, Koskenkorva P, Vanninen R, Lehesjoki AE, Kälviäinen R and Mervaala E. Altered cortical inhibition in Unverricht-Lundborg type progressive myoclonus epilepsy (EPM1). Epilepsy Res. 2009;85:81-88.

Danner N, Julkunen P, Könönen M, Hyppönen J, Koskenkorva P, Vanninen R, Lehesjoki AE, Kälviäinen R and Mervaala E. Primary motor cortex alterations in a compound heterozygous form of Unverricht-Lundborg disease (EPM1). Seizure 2011;20:65-71.

de Haan GJ, Halley DJ, Doelman JC, Geesink HH, Augustijn PB, Jager-Jongkind AD, Majoie M, Bader AJ, Leliefeld-Ten Doeschate LA, Deelen WH, Bertram E, Lehesjoki AE and Lindhout D. Univerricht-Lundborg disease: underdiagnosed in the Netherlands. Epilepsia 2004;45:1061-1063.

Deppe M, Kellinghaus C, Duning T, Moddel G, Mohammadi S, Deppe K, Schiffbauer H, Kugel H, Keller SS, Ringelstein EB and Knecht S. Nerve fiber impairment of anterior thalamocortical circuitry in juvenile myoclonic epilepsy. Neurology 2008;71:1981-1985.

Duvernoy, H.M. 1999, The Human Brain; Surface, Three-Dimensional Sectional Anatomy with MRI, and Blood Supply, 2nd edition edn, Springer-Verlag Wien.

Eldridge R, Iivanainen M, Stern R, Koerber T and Wilder BJ. "Baltic" myoclonus epilepsy: hereditary disorder of childhood made worse by phenytoin. Lancet 1983;2:838-842.

Erdinc O, Joensuu T, Ilgen-Uslu F, Bebek N, Özkara C, Tutkavul K, Gündüz A, Lehesjoki AE, Baykan B. Unverricht-Lundborg disease in Turkey: Delineating the phenotype between cystatin B mutation positive and negative cases. J Neurol Sci [Turk] 2010; 27: 001-011.

Fazekas F, Chawluk JB, Alavi A, Hurtig HI and Zimmerman RA. MR signal abnormalities at 1.5 T in Alzheimer's dementia and normal aging. AJR Am.J.Roentgenol. 1987;149:351-356.

Fellows GA, Wright AJ, Sibtain NA, Rich P, Opstad KS, McIntyre DJ, Bell BA, Griffiths JR and Howe FA. Combined use of neuroradiology and 1H-MR spectroscopy may provide an intervention limiting diagnosis of glioblastoma multiforme. J.Magn.Reson.Imaging 2010;32:1038-1044.

Ferlazzo E, Magaudda A, Striano P, Nguyen VH, Serra S and Genton P. Long-term evolution of EEG in Unverricht-Lundborg disease. Epilepsy Res. 2007;73:219-27.

Fischl B and Dale AM. Measuring the thickness of the human cerebral cortex from magnetic resonance images. Proc.Natl.Acad.Sci.U.S.A. 2000;97:11050-11055.

Fjell AM, Westlye LT, Amlien I, Espeseth T, Reinvang I, Raz N, Agartz I, Salat DH, Greve DN, Fischl B, Dale AM and Walhovd KB. High consistency of regional cortical thinning in aging across multiple samples. Cereb.Cortex 2009;19:2001-2012.

Focke NK. Correlation of cognitive functions with voxel-based morphometry in patients with hippocampal sclerosis. Epilepsy Behav 2008;12:472-476.

Focke NK, Yogarajah M, Bonelli SB, Bartlett PA, Symms MR and Duncan JS. Voxel-based diffusion tensor imaging in patients with mesial temporal lobe epilepsy and hippocampal sclerosis. Neuroimage 2008;40:728-737.

Forss N, Silen T and Karjalainen T. Lack of activation of human secondary somatosensory cortex in Unverricht-Lundborg type of progressive myoclonus epilepsy. Ann.Neurol. 2001;49:90-97.

Frucht SJ, Leurgans SE, Hallett M and Fahn S. The Unified Myoclonus Rating Scale. Adv.Neurol. 2002;89:361-376.

Gaetz W, Roberts TP, Singh KD and Muthukumaraswamy SD. Functional and structural correlates of the aging brain: Relating visual cortex (V1) gamma band responses to age-related structural change. Hum.Brain Mapp. 2011. (Epub ahead of print)

Gasparetto EL, Cabral RF, da Cruz LC,Jr and Domingues RC. Diffusion imaging in brain infections. Neuroimaging Clin.N.Am. 2011a;21:89-113, viii.

Gasparetto EL, Rueda Lopes FC, Domingues RC and Domingues RC. Diffusion imaging in traumatic brain injury. Neuroimaging Clin.N.Am. 2011b;21:115-25, viii.

Genovese CR, Lazar NA and Nichols T. Thresholding of statistical maps in functional neuroimaging using the false discovery rate. Neuroimage 2002;15:870-878.

Genton, P., Malafosse, A., Moulard, B., Rogel-Ortiz, F., Dravet, C., Bureau, M. & Roger, J. 2005, "Progressive myoclonus epilepsies" in Epileptic Syndromes in Infancy, Childhood and Adolescence, eds. J. Roger, M. Bureau, C. Dravet, P. Genton, C.A. Tassinari & P. Wolf, 4th edn. edn, John Libbey Eurotext Ltd, , pp. 441-465.

Genton P. Unverricht-Lundborg disease (EPM1). Epilepsia 2010;51 Suppl 1:37-39.

Genton P, Michelucci R, Tassinari CA and Roger J. The Ramsay Hunt syndrome revisited: Mediterranean myoclonus versus mitochondrial encephalomyopathy with ragged-red fibers and Baltic myoclonus. Acta Neurol.Scand. 1990;81:8-15.

Good C, Henson R, Friston K, Johnsrude I, Ashburner J and Frackowiak R. A voxel-based morphometric study of ageing in 465 normal adult human brains. Neuroimage 2001a;14:21-36.

Good CD, Ashburner J and Frackowiak RS. Computational neuroanatomy: new perspectives for neuroradiology. Rev.Neurol.(Paris) 2001b;157:797-806.

Good C, Johnsrude I, Ashburner J, Henson R, Friston K and Frackowiak R. Cerebral asymmetry and the effects of sex and handedness on brain structure: A voxel-based morphometric analysis of 465 normal adult human brains. Neuroimage 2001c;14:685-700.

Gore JC. Principles and practice of functional MRI of the human brain. J.Clin.Invest. 2003;112:4-9.

Haberg A, Kvistad KA, Unsgard G and Haraldseth O. Preoperative blood oxygen level-dependent functional magnetic resonance imaging in patients with primary brain tumors: clinical application and outcome. Neurosurgery 2004;54:902-914.

Haltia M, Kristensson K and Sourander P. Neuropathological studies in three Scandinavian cases of progressive myoclonus epilepsy. Acta Neurol.Scand. 1969;45:63-77.

Hämäläinen A, Pihlajamäki M, Tanila H, Hänninen T, Niskanen E, Tervo S, Karjalainen PA, Vanninen RL and Soininen H. Increased fMRI responses during encoding in mild cognitive impairment. Neurobiol.Aging 2007a;28:1889-1903.

Hämäläinen A, Tervo S, Grau-Olivares M, Niskanen E, Pennanen C, Huuskonen J, Kivipelto M, Hänninen T, Tapiola M, Vanhanen M, Hallikainen M, Helkala EL, Nissinen A, Vanninen R and Soininen H. Voxel-based morphometry to detect brain atrophy in progressive mild cognitive impairment. Neuroimage 2007b;37:1122-1131.

Henry TR and Votaw JR. The role of positron emission tomography with [18F]fluorodeoxyglucose in the evaluation of the epilepsies. Neuroimaging Clin.N.Am. 2004;14:517-535, ix.

Hyde KL, Samson F, Evans AC and Mottron L. Neuroanatomical differences in brain areas implicated in perceptual and other core features of autism revealed by cortical thickness analysis and voxel-based morphometry. Hum.Brain Mapp. 2010;31:556-566.

Hygino da Cruz LC,Jr, Vieira IG and Domingues RC. Diffusion MR imaging: an important tool in the assessment of brain tumors. Neuroimaging Clin.N.Am. 2011;21:27-49, vii.

Iivanainen M and Himberg JJ. Valproate and clonazepam in the treatment of severe progressive myoclonus epilepsy. Arch.Neurol. 1982;39:236-238.

Jenkinson M, Bannister P, Brady M and Smith S. Improved optimization for the robust and accurate linear registration and motion correction of brain images. Neuroimage 2002;17:825-841.

Jenkinson M and Smith S. A global optimisation method for robust affine registration of brain images. Med.Image Anal. 2001;5:143-156.

Joensuu T, Kuronen M, Alakurtti K, Tegelberg S, Hakala P, Aalto A, Huopaniemi L, Aula N, Michellucci R, Eriksson K and Lehesjoki AE. Cystatin B: mutation detection, alternative splicing and expression in progressive myclonus epilepsy of Unverricht-Lundborg type (EPM1) patients. Eur.J.Hum.Genet. 2007;15:185-193.

Joensuu T, Lehesjoki AE and Kopra O. Molecular background of EPM1-Unverricht-Lundborg disease. Epilepsia 2008;49:557-563.

Jones DK, Symms MR, Cercignani M and Howard RJ. The effect of filter size on VBM analyses of DT-MRI data. Neuroimage 2005;26:546-554.

Julkunen V, Niskanen E, Muehlboeck S, Pihlajamäki M, Könönen M, Hallikainen M, Kivipelto M, Tervo S, Vanninen R, Evans A and Soininen H. Cortical thickness analysis to detect progressive mild cognitive impairment: A reference to Alzheimer's disease. Dement.Geriatr.Cogn.Disord. 2009;28:404-412.

Khiari HM, Franceschetti S, Jovic N, Mrabet A and Genton P. Death in Unverricht-Lundborg disease. Neurol.Sci. 2009;30:315-318.

Kim, S. & Bandettini, P. 2006, "Principles of Functional MRI" in Functional MRI. Basic Principles and Clinical Applications, eds. S. Faro & F. Mohamed, Springer Science+Business Media, Inc., New York, pp. 3-23.

Kim JH, Lee JK, Koh SB, Lee SA, Lee JM, Kim SI and Kang JK. Regional grey matter abnormalities in juvenile myoclonic epilepsy: a voxel-based morphometry study. Neuroimage 2007;37:1132-1137.

Kim JS, Singh V, Lee JK, Lerch J, Ad-Dab'bagh Y, MacDonald D, Lee JM, Kim SI and Evans AC. Automated 3-D extraction and evaluation of the inner and outer cortical surfaces using a Laplacian map and partial volume effect classification. Neuroimage 2005;27:210-221.

Kokkonen SM, Nikkinen J, Remes J, Kantola J, Starck T, Haapea M, Tuominen J, Tervonen O and Kiviniemi V. Preoperative localization of the sensorimotor area using independent component analysis of resting-state fMRI. Magn.Reson.Imaging 2009;27:733-740.

Korja M, Kaasinen V, Lamusuo S, Marttila RJ and Parkkola R. Hyperostosis frontalis interna as a novel finding in Unverricht-Lundborg disease. Neurology 2007a;68:1077-1078.

Korja M, Kaasinen V, Lamusuo S, Parkkola R, Nagren K and Marttila RJ. Substantial thalamostriatal dopaminergic defect in Unverricht-Lundborg disease. Epilepsia 2007b;48:1768-1773.

Korja M, Ferlazzo E, Soilu-Hänninen M, Magaudda A, Marttila R, Genton P and Parkkola R. T2-weighted high-intensity signals in the basal ganglia as an interesting image finding in Unverricht-Lundborg disease. Epilepsy Res 2010; 88:87-91.

Koskiniemi M, Donner M, Majuri H, Haltia M and Norio R. Progressive myoclonus epilepsy. A clinical and histopathological study. Acta Neurol.Scand. 1974a;50:307-332.

Koskiniemi M, Toivakka E and Donner M. Progressive myoclonus epilepsy. Electroencephalographical findings. Acta Neurol.Scand. 1974b;50:333-359.

Kälviäinen R, Khyuppenen J, Koskenkorva P, Eriksson K, Vanninen R and Mervaala E. Clinical picture of EPM1-Unverricht-Lundborg disease. Epilepsia 2008;49:549-56.

Lafreniere RG, Rochefort DL, Chretien N, Rommens JM, Cochius JI, Kälviäinen R, Nousiainen U, Patry G, Farrell K, Soderfeldt B, Federico A, Hale BR, Cossio OH, Sorensen T, Pouliot MA, Kmiec T, Uldall P, Janszky J, Pranzatelli MR, Andermann F, Andermann E and Rouleau GA. Unstable insertion in the 5' flanking region of the cystatin B gene is the most common mutation in progressive myoclonus epilepsy type 1, EPM1. Nat.Genet. 1997;15:298-302.

Lalioti MD, Mirotsou M, Buresi C, Peitsch MC, Rossier C, Ouazzani R, Baldy-Moulinier M, Bottani A, Malafosse A and Antonarakis SE. Identification of mutations in cystatin B, the gene responsible for the Unverricht-Lundborg type of progressive myoclonus epilepsy (EPM1). Am.J.Hum.Genet. 1997a;60:342-351.

Lalioti MD, Scott HS, Buresi C, Rossier C, Bottani A, Morris MA, Malafosse A and Antonarakis SE. Dodecamer repeat expansion in cystatin B gene in progressive myoclonus epilepsy. Nature 1997b;386:847-851.

Lalioti MD, Scott HS, Genton P, Grid D, Ouazzani R, M'Rabet A, Ibrahim S, Gouider R, Dravet C, Chkili T, Bottani A, Buresi C, Malafosse A and Antonarakis SE. A PCR amplification method reveals instability of the dodecamer repeat in progressive myoclonus epilepsy (EPM1) and no correlation between the size of the repeat and age at onset. Am.J.Hum.Genet. 1998;62:842-847.

Lancaster JL, Woldorff MG, Parsons LM, Liotti M, Freitas CS, Rainey L, Kochunov PV, Nickerson D, Mikiten SA and Fox PT. Automated Talairach atlas labels for functional brain mapping. Hum.Brain Mapp. 2000;10:120-131.

Lee JK, Lee JM, Kim JS, Kim IY, Evans AC and Kim SI. A novel quantitative cross-validation of different cortical surface reconstruction algorithms using MRI phantom. Neuroimage 2006;31:572-584.

Lehesjoki AE, Eldridge R, Eldridge J, Wilder BJ and de la Chapelle A. Progressive myoclonus epilepsy of Unverricht-Lundborg type: a clinical and molecular genetic study of a family from the United States with four affected sibs. Neurology 1993;43:2384-2386.

Lerch JP and Evans AC. Cortical thickness analysis examined through power analysis and a population simulation. Neuroimage 2005a;24:163-173.

Lerch JP, Pruessner JC, Zijdenbos A, Hampel H, Teipel SJ and Evans AC. Focal decline of cortical thickness in Alzheimer's disease identified by computational neuroanatomy. Cereb.Cortex 2005b;15:995-1001.

Li R, Wu X, Fleisher AS, Reiman EM, Chen K and Yao L. Attention-related networks in Alzheimer's disease: A resting functional MRI study. Hum.Brain Mapp. 2011. (Epub ahead of print)

Liu Y, Spulber G, Lehtimäki KK, Könönen M, Hallikainen I, Gröhn H, Kivipelto M, Hallikainen M, Vanninen R and Soininen H. Diffusion tensor imaging and Tract-Based Spatial Statistics in Alzheimer's disease and mild cognitive impairment. Neurobiol.Aging 2011;32:1558-1571.

Lundborg H. Die progressive Myoclonus-Epilepsie (Unverricht's Myoclonie). 1903.

Lötjönen J, Wolz R, Koikkalainen J, Julkunen V, Thurfjell L, Lundqvist R, Waldemar G, Soininen H, Rueckert D and the Alzheimer's Disease Neuroimaging Initiative. Fast and robust extraction of hippocampus from MR images for diagnostics of Alzheimer's disease. Neuroimage 2011;56:185-196.

MacDonald D, Kabani N, Avis D and Evans AC. Automated 3-D extraction of inner and outer surfaces of cerebral cortex from MRI. Neuroimage 2000;12:340-356.

Magaudda A, Ferlazzo E, Nguyen VH and Genton P. Unverricht-Lundborg disease, a condition with self-limited progression: long-term follow-up of 20 patients. Epilepsia 2006;47:860-866.

Majos C, Aguilera C, Alonso J, Julia-Sape M, Castaner S, Sanchez JJ, Samitier A, Leon A, Rovira A and Arus C. Proton MR spectroscopy improves discrimination between tumor and pseudotumoral lesion in solid brain masses. AJNR Am.J.Neuroradiol. 2009;30:544-551.

Manganotti P, Brigo F, Zoccatelli G, Alessandrini F, Pizzini FB, Beltramello A, Storti S, Formaggio E, Fiaschi A and Bongiovanni LG. Highly focal BOLD activation on functional MRI in a patient with progressive myoclonic epilepsy and diffuse giant somatosensory evoked potentials. Epilepsy Behav. 2011;20:579-582.

Mangin JF, Frouin V, Bloch I, Regis J and Lopez-Krahe J. From 3D MR images to structural representations of the cortex topography using topology preserving deformations. J Math Imaging Vis 1995;5:297-318.

Mascalchi M, Michelucci R, Cosottini M, Tessa C, Lolli F, Riguzzi P, Lehesjoki AE, Tosetti M, Villari N and Tassinari CA. Brainstem involvement in Unverricht-Lundborg disease (EPM1): An MRI and 1H MRS study. Neurology 2002;58:1686-1689.

Mascalchi M, Tessa C, Bartolozzi C, Bianchi MC, Frontali M, Tosetti M, Plasmati R, Salvi F and Valzania F. Proton magnetic resonance spectroscopy in an Italian family with spinocerebellar ataxia type 1. Ann.Neurol. 1998a;43:244-252.

Mascalchi M, Tosetti M, Plasmati R, Bianchi MC, Tessa C, Salvi F, Frontali M, Valzania F, Bartolozzi C and Tassinari CA. Proton magnetic resonance spectroscopy in an Italian family with spinocerebellar ataxia type 1. Ann.Neurol. 1998b;43:244-252.

Mazziotta J, Toga A, Evans A, Fox P, Lancaster J, Zilles K, Woods R, Paus T, Simpson G, Pike B, Holmes C, Collins L, Thompson P, MacDonald D, Iacoboni M, Schormann T, Amunts K, Palomero-Gallagher N, Geyer S, Parsons L, Narr K, Kabani N, Le Goualher G, Boomsma D, Cannon T, Kawashima R and Mazoyer B. A probabilistic atlas and reference system for the human brain: International Consortium for Brain Mapping (ICBM). Philos.Trans.R.Soc.Lond.B.Biol.Sci. 2001;356:1293-1322.

Medina MT, Martinez-Juarez IE, Duron RM, Genton P, Guerrini R, Dravet C, Bureau M, Perez-Gosiengfiao KT, Amador C, Bailey JN, Chaves-Sell F and Delgado-Escueta AV. Treatment of myoclonic epilepsies of childhood, adolescence, and adulthood. Adv.Neurol. 2005;95:307-323.

Mervaala E, Keränen T, Paakkonen A, Partanen JV and Riekkinen P. Visual evoked potentials, brainstem auditory evoked potentials, and quantitative EEG in Baltic progressive myoclonus epilepsy. Epilepsia 1986;27:542-547.

Mervaala E, Partanen JV, Keränen T, Penttilä M and Riekkinen P. Prolonged cortical somatosensory evoked potential latencies in progressive myoclonus epilepsy. J.Neurol.Sci. 1984;64:131-135.

Mesulam MM. From sensation to cognition. Brain 1998;121 (Pt 6):1013-1052.

Mezzapesa DM, Ceccarelli A, Dicuonzo F, Carella A, De Caro MF, Lopez M, Samarelli V, Livrea P and Simone IL. Whole-brain and regional brain atrophy in amyotrophic lateral sclerosis. AJNR Am.J.Neuroradiol. 2007;28:255-9.

Mima T, Nagamine T, Ikeda A, Yazawa S, Kimura J and Shibasaki H. Pathogenesis of cortical myoclonus studied by magnetoencephalography. Ann.Neurol. 1998a;43:598-607.

Mima T, Nagamine T, Nishitani N, Mikuni N, Ikeda A, Fukuyama H, Takigawa T, Kimura J and Shibasaki H. Cortical myoclonus: sensorimotor hyperexcitability. Neurology 1998b;50:933-942.

Mori S, Crain BJ, Chacko VP and van Zijl PC. Three-dimensional tracking of axonal projections in the brain by magnetic resonance imaging. Ann.Neurol. 1999;45:265-269.

Moulard B, Genton P, Grid D, Jeanpierre M, Ouazzani R, Mrabet A, Morris M, LeGuern E, Dravet C, Mauguiere F, Utermann B, Baldy-Moulinier M, Belaidi H, Bertran F, Biraben A, Ali Cherif A, Chkili T, Crespel A, Darcel F, Dulac O, Geny C, Humbert-Claude V, Kassiotis

P, Buresi C and Malafosse A. Haplotype study of West European and North African Unverricht-Lundborg chromosomes: evidence for a few founder mutations. Hum.Genet. 2002;111:255-262.

Norio R and Koskiniemi M. Progressive myoclonus epilepsy: genetic and nosological aspects with special reference to 107 Finnish patients. Clin.Genet. 1979;15:382-398.

Paakki JJ, Rahko J, Long X, Moilanen I, Tervonen O, Nikkinen J, Starck T, Remes J, Hurtig T, Haapsamo H, Jussila K, Kuusikko-Gauffin S, Mattila ML, Zang Y and Kiviniemi V. Alterations in regional homogeneity of resting-state brain activity in autism spectrum disorders. Brain Res. 2010;1321:169-179.

Parmeggiani A, Lehesjoki AE, Carelli V, Posar A, Santi A, Santucci M, Gobbi G, Pini A and Rossi PG. Familial Unverricht-Lundborg disease: a clinical, neurophysiologic, and genetic study. Epilepsia 1997;38:637-641.

Pennacchio LA, Bouley DM, Higgins KM, Scott MP, Noebels JL and Myers RM. Progressive ataxia, myoclonic epilepsy and cerebellar apoptosis in cystatin B-deficient mice. Nat.Genet. 1998;20:251-258.

Pennacchio LA, Lehesjoki AE, Stone NE, Willour VL, Virtaneva K, Miao J, D'Amato E, Ramirez L, Faham M, Koskiniemi M, Warrington JA, Norio R, de la Chapelle A, Cox DR and Myers RM. Mutations in the gene encoding cystatin B in progressive myoclonus epilepsy (EPM1). Science 1996;271:1731-1734.

Pierpaoli C and Basser PJ. Toward a quantitative assessment of diffusion anisotropy. Magn.Reson.Med. 1996;36:893-906.

Richards T, Stevenson J, Crouch J, Johnson LC, Maravilla K, Stock P, Abbott R and Berninger V. Tract-based spatial statistics of diffusion tensor imaging in adults with dyslexia. AJNR Am.J.Neuroradiol.2008;29:1134-1139.

Roberts TP and Schwartz ES. Principles and implementation of diffusion-weighted and diffusion tensor imaging. Pediatr.Radiol. 2007;37:739-748.

Sage CA, Peeters RR, Gorner A, Robberecht W and Sunaert S. Quantitative diffusion tensor imaging in amyotrophic lateral sclerosis. Neuroimage 2007;34:486-499.

Salat DH, Buckner RL, Snyder AZ, Greve DN, Desikan RS, Busa E, Morris JC, Dale AM and Fischl B. Thinning of the cerebral cortex in aging. Cereb.Cortex 2004;14:721-730.

Santoshkumar B, Turnbull J and Minassian BA. Unverricht-Lundborg progressive myoclonus epilepsy in Oman. Pediatr.Neurol. 2008;38:252-5.

Scheinin NM, Aalto S, Koikkalainen J, Lötjönen J, Karrasch M, Kemppainen N, Viitanen M, Nagren K, Helin S, Scheinin M and Rinne JO. Follow-up of [11C]PIB uptake and brain volume in patients with Alzheimer disease and controls. Neurology 2009;73:1186-1192.

Shahwan A, Farrell M and Delanty N. Progressive myoclonic epilepsies: a review of genetic and therapeutic aspects. Lancet Neurol. 2005;4:239-248.

Shannon P, Pennacchio LA, Houseweart MK, Minassian BA and Myers RM. Neuropathological changes in a mouse model of progressive myoclonus epilepsy: cystatin

B deficiency and Unverricht-Lundborg disease. J.Neuropathol.Exp.Neurol. 2002;61:1085-1091.

Shellock FG, Morisoli S and Kanal E. MR procedures and biomedical implants, materials, and devices: 1993 update. Radiology 1993;189:587-599.
Shields WD. Diagnosis of infantile spasms, Lennox-Gastaut syndrome, and progressive myoclonic epilepsy. Epilepsia 2004;45 Suppl 5:2-4.

Sicotte NL, Kern KC, Giesser BS, Arshanapalli A, Schultz A, Montag M, Wang H and Bookheimer SY. Regional hippocampal atrophy in multiple sclerosis. Brain 2008;131:1134-1141.

Silen T, Forss N, Jensen O and Hari R. Abnormal reactivity of the approximately 20-Hz motor cortex rhythm in Unverricht Lundborg type progressive myoclonus epilepsy. Neuroimage 2000;12:707-712.

Silen T, Forss N, Salenius S, Karjalainen T and Hari R. Oscillatory cortical drive to isometrically contracting muscle in Unverricht-Lundborg type progressive myoclonus epilepsy (ULD). Clin.Neurophysiol. 2002a;113:1973-1979.

Silen T, Karjalainen T, Lehesjoki AE and Forss N. Cortical sensorimotor alterations in Unverricht-Lundborg disease patients without generalized seizures. Neurosci.Lett. 2002b;323:101-104.

Simon TJ, Ding L, Bish JP, McDonald-McGinn DM, Zackai EH and Gee J. Volumetric, connective, and morphologic changes in the brains of children with chromosome 22q11.2 deletion syndrome: an integrative study. Neuroimage 2005;25:169-180.

Skoch A, Jiru F and Bunke J. Spectroscopic imaging: basic principles. Eur.J.Radiol. 2008;67:230-239.

Sled JG, Zijdenbos AP and Evans AC. A nonparametric method for automatic correction of intensity nonuniformity in MRI data. IEEE Trans.Med.Imaging 1998;17:87-97.

Smith SM, Jenkinson M, Johansen-Berg H, Rueckert D, Nichols TE, Mackay CE, Watkins KE, Ciccarelli O, Cader MZ, Matthews PM and Behrens TE. Tract-based spatial statistics: voxelwise analysis of multi-subject diffusion data. Neuroimage 2006;31:1487-1505.

Smith SM, Johansen-Berg H, Jenkinson M, Rueckert D, Nichols TE, Miller KL, Robson MD, Jones DK, Klein JC, Bartsch AJ and Behrens TE. Acquisition and voxelwise analysis of multi-subject diffusion data with tract-based spatial statistics. Nat.Protoc. 2007;2:499-503.

Smith SM and Nichols TE. Threshold-free cluster enhancement: addressing problems of smoothing, threshold dependence and localisation in cluster inference. Neuroimage 2009;44:83-98.

Soininen HS, Partanen K, Pitkänen A, Vainio P, Hänninen T, Hallikainen M, Koivisto K and Riekkinen PJ S. Volumetric MRI analysis of the amygdala and the hippocampus in subjects with age-associated memory impairment: correlation to visual and verbal memory. Neurology 1994;44:1660-1668.

Song SK, Sun SW, Ju WK, Lin SJ, Cross AH and Neufeld AH. Diffusion tensor imaging detects and differentiates axon and myelin degeneration in mouse optic nerve after retinal ischemia. Neuroimage 2003;20:1714-1722.

Song SK, Yoshino J, Le TQ, Lin SJ, Sun SW, Cross AH and Armstrong RC. Demyelination increases radial diffusivity in corpus callosum of mouse brain. Neuroimage 2005;26:132-140.

Spencer MD, Moorhead TWJ, McIntosh AM, Stanfield AC, Muir WJ, Hoare P, Owens DGC, Lawrie SM and Johnstone EC. Grey matter correlates of early psychotic symptoms in adolescents at enhanced risk of psychosis: A voxel-based study. NeuroImage 2007;35:1181-1191.

Sun SW, Liang HF, Cross AH and Song SK. Evolving Wallerian degeneration after transient retinal ischemia in mice characterized by diffusion tensor imaging. Neuroimage 2008;40:1-10.

Tamraz JC, Comair YG, 2006. Atlas of Regional Anatomy of the Brain Using MRI with Functional Correlations, Springer-Verlag Berlin Heidelberg New York.

Tatsch K. Extrapyramidal syndromes: PET and SPECT. Neuroimaging Clin.N.Am. 2010;20:57-68.

Teipel SJ, Meindl T, Grinberg L, Heinsen H and Hampel H. Novel MRI techniques in the assessment of dementia. Eur.J.Nucl.Med.Mol.Imaging 2008;35 Suppl 1:S58-69.

Thambisetty M, Wan J, Carass A, An Y, Prince JL and Resnick SM. Longitudinal changes in cortical thickness associated with normal aging. Neuroimage 2010;52:1215-1223.

Thivard L, Pradat PF, Lehericy S, Lacomblez L, Dormont D, Chiras J, Benali H and Meininger V. Diffusion tensor imaging and voxel based morphometry study in amyotrophic lateral sclerosis: relationships with motor disability. J.Neurol.Neurosurg.Psychiatry. 2007;78:889-892.

Tijssen MA, Thom M, Ellison DW, Wilkins P, Barnes D, Thompson PD and Brown P. Cortical myoclonus and cerebellar pathology. Neurology 2000;54:1350-1356.

Tohka J, Zijdenbos A and Evans A. Fast and robust parameter estimation for statistical partial volume models in brain MRI. Neuroimage 2004;23:84-97.

Unverricht H. Die Myoclonie. 1891.

Virtaneva K, D'Amato E, Miao J, Koskiniemi M, Norio R, Avanzini G, Franceschetti S, Michelucci R, Tassinari CA, Omer S, Pennacchio LA, Myers RM, Dieguez-Lucena JL, Krahe R, de la Chapelle A and Lehesjoki AE. Unstable minisatellite expansion causing recessively inherited myoclonus epilepsy, EPM1. Nat.Genet. 1997;15:393-396.

Visani E, Agazzi P, Canafoglia L, Panzica F, Ciano C, Scaioli V, Avanzini G and Franceschetti S. Movement-related desynchronization-synchronization (ERD/ERS) in patients with Unverricht-Lundborg disease. Neuroimage 2006;33:161-168.

Visani E, Minati L, Canafoglia L, Gilioli I, Granvillano A, Varotto G, Aquino D, Fazio P, Bruzzone MG, Franceschetti S and Panzica F. Abnormal ERD/ERS but unaffected BOLD response in patients with Unverricht-Lundborg disease during index extension: a simultaneous EEG-fMRI study. Brain Topogr. 2011;24:65-77.

Visani E, Minati L, Canafoglia L, Gilioli I, Salvatoni L, Varotto G, Fazio P, Aquino D, Bruzzone MG, Franceschetti S and Panzica F. Simultaneous EEG-fMRI in patients with Unverricht-Lundborg disease: event-related desynchronization/synchronization and hemodynamic response analysis. Comput.Intell.Neurosci.2010. (Epub ahead of print)

Walz NC, Cecil KM, Wade SL and Michaud LJ. Late proton magnetic resonance spectroscopy following traumatic brain injury during early childhood: relationship with neurobehavioral outcomes. J.Neurotrauma 2008;25:94-103.

Wechsler, D. 1981, Wechsler Adult Intelligence Scale - Revised, Psychological Corp, New York, NY.

Weybright P, Sundgren PC, Maly P, Hassan DG, Nan B, Rohrer S and Junck L. Differentiation between brain tumor recurrence and radiation injury using MR spectroscopy. AJR Am.J.Roentgenol. 2005;185:1471-1476.

Wolz R, Julkunen V, Koikkalainen J, Niskanen E, Zhang DP, Rueckert D, Soininen H, Lötjönen J and the Alzheimer's Disease Neuroimaging Initiative. Multi-method analysis of MRI images in early diagnostics of Alzheimer's disease. PLoS One 2011;6:e25446.

Yamashita K, Yoshiura T, Hiwatashi A, Kamano H, Dashjamts T, Shibata S, Tamae A and Honda H. Detection of middle ear cholesteatoma by diffusion-weighted MR imaging: Multishot echo-planar imaging compared with single-shot echo-planar imaging. AJNR Am.J.Neuroradiol. 2011;32:1915-1918.

Yang E, Nucifora PG and Melhem ER. Diffusion MR imaging: basic principles. Neuroimaging Clin.N.Am. 2011;21:1-25, vii.

Yoo AJ and Gonzalez RG. Clinical applications of diffusion MR imaging for acute ischemic stroke. Neuroimaging Clin.N.Am. 2011;21:51-69, vii.

Yoshida T, McCarley RW, Nakamura M, Lee K, Koo MS, Bouix S, Salisbury DF, Morra L, Shenton ME and Niznikiewicz MA. A prospective longitudinal volumetric MRI study of superior temporal gyrus gray matter and amygdala-hippocampal complex in chronic schizophrenia. Schizophr.Res. 2009;113:84-94.

Zijdenbos AP, Forghani R and Evans AC. Automatic "pipeline" analysis of 3-D MRI data for clinical trials: application to multiple sclerosis. IEEE Trans.Med.Imaging 2002;21:1280-1291.

Päivi Koskenkorva

Magnetic Resonance Imaging of Unverricht-Lundborg Disease (EPM1)

Modern MR imaging techniques and analysis methods voxel-based morphometry (VBM), cortical thickness analysis and diffusion tensor imaging (DTI) enable detailed evaluation of gray matter (GM) and white matter (WM) structures of the brain. In this study the combination of these methods revealed previously undetected extensive changes both in GM and WM of patients with Unverricht-Lundborg disease (EPM1), the most common form of progressive myoclonus epilepsy. The changes parallel the symptoms of EPM1 and explain the poor response to antiepileptic drug treatment.

UNIVERSITY OF EASTERN FINLAND

Publications of the University of Eastern Finland
Dissertations in Health Sciences

ISBN 978-952-61-0687-8